

PDF hosted at the Radboud Repository of the Radboud University Nijmegen

The following full text is a publisher's version.

For additional information about this publication click this link.

<http://hdl.handle.net/2066/28060>

Please be advised that this information was generated on 2018-10-16 and may be subject to change.

Soft two-meson-exchange nucleon-nucleon potentials. I. Planar and crossed-box diagrams

Th. A. Rijken

Institute for Theoretical Physics, University of Nijmegen, Nijmegen, The Netherlands

V. G. J. Stoks*

Department of Physics, The Flinders University of South Australia, Bedford Park, South Australia 5042, Australia

(Received 1 September 1995)

Pion-meson-exchange nucleon-nucleon potentials are derived for two nucleons in the intermediate states. The mesons we include are (i) pseudoscalar mesons π , η , and η' , (ii) vector mesons ρ , ω , and ϕ , (iii) scalar mesons $a_0(980)$, $\varepsilon(760)$, and $f_0(975)$, and (iv) the $J=0$ contribution from the Pomeron. Strong dynamical pair suppression is assumed, and at the nucleon-nucleon-meson vertices Gaussian form factors are incorporated into the relativistic two-body framework using a dispersion representation for the pion- and meson-exchange amplitudes. The Fourier transformations are performed using factorization techniques for the energy denominators. The potentials are first calculated in the adiabatic approximation to all planar and crossed three-dimensional momentum-space π -meson diagrams. Next, we calculate the $1/M$ corrections. [S0556-2813(96)02912-3]

PACS number(s): 13.75.Cs, 12.39.Pn, 21.30.-x

I. INTRODUCTION

This paper and its companion paper [1] are part of our program to extend the Nijmegen soft-core one-boson-exchange potential [2] by including two-meson-exchange potentials. The material presented here is incorporated into a new extended soft-core (ESC) nucleon-nucleon model, hereafter referred to as the ESC potential. We are still investigating ways to improve this model as much as possible, but the preliminary version of the ESC potential employed in the present paper is here used to illustrate the contributions of the various two-meson exchanges.

In low-energy nucleon-nucleon models, exchanges with an effective mass less than 1 GeV seem to be the most important ones. The very heavy mesons possibly only play some role for S waves, but they can presumably be covered up by the lower-mass mesons. After one-meson exchange, the effects of two-meson exchanges at low energies seem worthwhile to be investigated and, as we will demonstrate with the ESC potential, they indeed provide a major improvement in the theoretical description of the nucleon-nucleon data.

Recently, we have evaluated the soft two-pion-exchange potentials in coordinate space, using some new techniques [3]. We noted that these techniques could also be applied to double-meson exchanges where the mesons have different masses. For the double-meson exchanges we can distinguish two different classes. The first class consists of the diagrams with two baryons (nucleons) in the intermediate states, which can be simply understood as the second-order contributions in a series expansion of multi-meson exchanges. In this paper we calculate these two-meson-exchange (TME) potentials, using Gaussian form factors, for the cases where one of the exchanged mesons is the pion. For exchanges with effec-

tive masses below 1 GeV these are the most important ones. An extension to the most general two-meson exchange (not necessarily involving at least one pion) can then be evaluated in a straightforward manner. Furthermore, we restrict ourselves to the case with two nucleons in the intermediate states. The potentials containing the isobar excitation effects explicitly have been considered elsewhere [4,5].

The second class consists of the diagrams where either one or both nucleons contains a pair vertex ("seagull" diagrams). The pair-meson diagrams can be viewed as the result of integrating out the heavy-meson and resonance degrees of freedom in the two-meson-exchange processes (see, e.g., Ref. [6]). It will appear that these "seagull" contributions can be interpreted successfully in a "dual" picture [7]. The various possibilities for meson pairs coupling to the nucleon are inspired by the chiral-invariant phenomenological Lagrangians that have appeared in the literature. The pair-meson potentials belonging to this second class will be presented in the companion paper [1].

The mesons we include are (i) pseudoscalar mesons π , η , and η' , (ii) vector mesons ρ , ω , and ϕ , (iii) scalar mesons [8] $a_0(980)$, $\varepsilon(760)$, and $f_0(975)$, and (iv) the $J=0$ contribution from the Pomeron. The 2π -exchange potential has already been derived in Ref. [3], and we here only include those results for reasons of completeness. In the literature, the treatment of two-meson exchanges is incomplete. For example, the $\pi\omega$ potential has been derived in the dispersion-relation approach [9], which does not allow for the inclusion of Gaussian form factors as applied in the present study. For the $\pi\omega$, $\pi\rho$, and $\pi\sigma$ exchanges, only the noniterative potentials from the graphs with at least one meson in the intermediate state (see below) have been evaluated in momentum space in the framework of noncovariant perturbation theory [10]. In this paper we give, apart from the 2π exchange, the potentials for all pion-meson exchanges with a total mass less than ~ 1 GeV.

Our general approach to two-meson-exchange potentials is given, in principle, in Ref. [3]. Starting from the relativis-

*Present address: TRIUMF, 4004 Wesbrook Mall, Vancouver, British Columbia, Canada V6T 2A3.

tic two-body equations, the two-meson-exchange potentials for the relativistic three-dimensional integral equation and for the Lippmann-Schwinger equation are derived from the second-order Feynman diagrams by integration over the relative energies [11]. This way, the ‘‘old-fashioned’’ perturbation graphs for the TME potentials are obtained from the Feynman diagrams.

The proper way to incorporate Gaussian form factors is explained in [3] and, as already mentioned above, in this paper the important ‘‘factorization’’ technique involving two mesons with different masses will be exploited. It is in particular this factorization technique which enables us to express the two-meson exchanges in terms of the basic coordinate-space function $\phi_C^0(r)$ of the Nijmegen one-boson-exchange (OBE) model [2,12,13]. Technically, there is no compelling reason to work in coordinate space, rather than in momentum space. Electromagnetic effects can be included more easily in coordinate space, whereas relativistic effects can be studied more effectively in momentum space. However, we think that at low energies relativistic effects can be included sufficiently accurate in coordinate space. Coordinate-space interactions are useful, for example, in Jastrow variational calculations (see, e.g., Refs. [14,15]) or in applications where one wishes to distinguish a (long-range) meson-exchange region and a (short-range) quark-exchange region (see, e.g., Refs. [16,17]). Furthermore, the effect of the particular shape of the central, spin-spin, tensor, and spin-orbit components on the phase shifts is much more transparent in a coordinate-space picture. Ultimately, it is our goal to produce an NN potential which is exactly equivalent in both coordinate space and momentum space.

The graphs which we calculate are (i) the planar and crossed π -meson-exchange graphs of a similar type as those calculated by Brueckner and Watson (BW) [18] for two-pion exchange and (ii) the iterated π -meson-exchange graphs of the type of graphs calculated by Taketani, Machida, and Ohnuma (TMO) [19] for two-pion exchange. As the distinction between these two classes of graphs is convenient as a means to denote the different contributions, we will also adopt in this paper the following nomenclature: The noniterative potential graphs with at least one meson in the intermediate state are of class (i) and will be referred to as planar (//) and crossed (X) BW graphs, while the iterative graphs with only nucleons in the intermediate state are of class (ii) and will be referred to as TMO graphs.

The π -meson-exchange potentials are calculated first using the adiabatic approximation for the nucleons in the intermediate states. However, in the meson exchanges we include the $1/M^2$ terms, in analogy with the OBE model [2,12,13]. We find that up to this order the $\pi\varepsilon$ and πf_0 potentials are identically zero. Also, in the π -vector and π -pseudoscalar potentials there are large cancellations between the contributions from the planar and crossed-box diagrams when the meson is an isoscalar ($I=0$) meson. Therefore, the next to leading order is expected to be important, and so we here also calculate the nonadiabatic $1/M$ corrections and the $1/M$ corrections from the pseudovector coupling of the pion and the other pseudoscalar mesons.

The paper is organized as follows. In Sec. II we define the two-meson-exchange kernels. We give the interaction Hamiltonians and briefly indicate how the Gaussian form

factors can be implemented. In Sec. III the definition of the nucleon-nucleon two-meson potential for the Lippmann-Schwinger equation is briefly repeated from [3] and the vertices in Pauli-spinor space for the different couplings are given. Here we also mention the approximations made in these vertices. In the next section, the π -pseudoscalar, the π -scalar, the π -Pomeron, and the π -vector potentials are derived. In Sec. V we derive the $1/M$ corrections, due to (i) the nonadiabatic corrections, (ii) the $1/M$ term in the pseudovector coupling of the pion and the other pseudoscalar mesons, and (iii) a cancellation between the $1/M^2$ off-shell term in the pseudovector vertices and the $1/M$ term of the two-nucleon intermediate state in the TMO diagrams. In Sec. VI the results are shown and discussed.

Appendix A contains a dictionary of differentiation formulas, adequate for deriving the final form of the potentials of this paper in coordinate space. Explicit expressions for the leading-order contributions to the coordinate-space potentials are given in Appendix B.

II. TWO-MESON-EXCHANGE KERNEL

The fourth-order two-meson-exchange kernel is derived following the procedure as discussed in [5], to which we refer for details and definitions. The only difference is that here we choose to shift the M/E factors into the Green’s function. This means that the Thompson equation reads

$$\begin{aligned} \phi_{++}(\mathbf{p}') &= \phi_{++}^{(0)}(\mathbf{p}') + E_2^{(+)}(\mathbf{p}'; W) \\ &\times \int d^3p K^{\text{irr}}(\mathbf{p}', \mathbf{p} | W) \phi_{++}(\mathbf{p}), \end{aligned} \quad (2.1)$$

where now the Green’s function is

$$E_2^{(+)}(\mathbf{p}'; W) = \frac{1}{(2\pi)^3} \left[\frac{M_a M_b}{E_a(\mathbf{p}') E_b(\mathbf{p}')} \right] \frac{\Lambda_+^a(\mathbf{p}') \Lambda_+^b(-\mathbf{p}')}{W - \mathcal{W}(\mathbf{p}') + i\delta}, \quad (2.2)$$

and so the irreducible kernel is then given by

$$\begin{aligned} K^{\text{irr}}(\mathbf{p}', \mathbf{p} | W) &= -(2\pi)^{-2} [W - \mathcal{W}(\mathbf{p}')] \\ &\times [W - \mathcal{W}(\mathbf{p})] \int_{-\infty}^{\infty} dp'_0 \int_{-\infty}^{\infty} dp_0 \\ &\times \{ [F_W^{(a)}(\mathbf{p}', p'_0) F_W^{(b)}(-\mathbf{p}', -p'_0)]^{-1} \\ &\times [I(p'_0, \mathbf{p}'; p_0, \mathbf{p})]_{++,++} \\ &\times [F_W^{(a)}(\mathbf{p}, p_0) F_W^{(b)}(-\mathbf{p}, -p_0)]^{-1} \}. \end{aligned} \quad (2.3)$$

The transition from the Thompson equation (2.1) to the Lippmann-Schwinger equation,

$$\phi(\mathbf{p}') = \phi^{(0)}(\mathbf{p}') + g(\mathbf{p}'; W) \int d^3p V(\mathbf{p}', \mathbf{p} | W) \phi(\mathbf{p}), \quad (2.4)$$

is effectuated by the transformations

$$\phi_{++}(\mathbf{p}) = N(\mathbf{p}; W) \phi(\mathbf{p}),$$

$$K^{\text{irr}}(\mathbf{p}', \mathbf{p} | W) = N^{-1}(\mathbf{p}'; W) V(\mathbf{p}', \mathbf{p} | W) N^{-1}(\mathbf{p}; W),$$

$$E_2^{(+)}(\mathbf{p}; W) = N^2(\mathbf{p}; W) g(\mathbf{p}; W), \quad (2.5)$$

with the nonrelativistic Green's function

$$g(\mathbf{p}; W) = \frac{1}{(2\pi)^3} \Lambda_+^a(\mathbf{p}) \Lambda_+^b(-\mathbf{p}) \frac{M}{\mathbf{p}_i^2 - \mathbf{p}^2 + i\delta}, \quad (2.6)$$

where \mathbf{p}_i is the on-shell momentum. For NN scattering the equal-mass approximation is very nearly valid. In that case we have, taking the nucleons on the energy shell,

$$N(\mathbf{p}; W) = \sqrt{M/E(\mathbf{p})}. \quad (2.7)$$

Taking further into account the normalization factors of the nucleon Dirac spinors, it is then natural to write

$$V(\mathbf{p}', \mathbf{p}) = \sqrt{\frac{M}{E(\mathbf{p}')}} \left(\frac{E(\mathbf{p}') + M}{2M} \right) U(\mathbf{p}', \mathbf{p}) \\ \times \left(\frac{E(\mathbf{p}) + M}{2M} \right) \sqrt{\frac{M}{E(\mathbf{p})}}$$

$$\approx U(\mathbf{p}', \mathbf{p}) [1 + \mathcal{O}(1/M^4)], \quad (2.8)$$

where the potential function $U(\mathbf{p}', \mathbf{p})$ has a reduced energy dependence.

The two-meson-exchange kernel is written as a power series in λ , which denotes the number of nucleon-nucleon-meson (NNm) vertices. The various two-meson contributions to the fourth-order λ terms of the two-meson-exchange (TME) kernel define the various two-meson-exchange potentials. The corresponding fourth-order elastic NN matrix element of the kernel now reads

$$K^{(4)}(\mathbf{p}', \mathbf{p} | W)_{a'b'; ab} = -(2\pi)^{-2} [W - \mathcal{W}(\mathbf{p}')] [W - \mathcal{W}(\mathbf{p})] \sum_{a'', b''} \int dp'_0 \int dp_0 \int dk_{10} \int dk_{20} \int d\mathbf{k}_1 \int d\mathbf{k}_2 i(2\pi)^{-4} \\ \times \delta^4(p' - p - k_1 - k_2) [k_2^2 - m_2^2 + i\delta]^{-1} [F_W^{(a')}(\mathbf{p}', p'_0) F_W^{(b')}(-\mathbf{p}', -p'_0)]^{-1} \\ \times \{ [\Gamma_j F_W^{-1}(\mathbf{p} + \mathbf{k}_1, p_0 + k_{10}) \Gamma_i]^{(a'')} [\Gamma_j F_W^{-1}(-\mathbf{p} - \mathbf{k}_1, -p_0 - k_{10}) \Gamma_i]^{(b'')} \\ + [\Gamma_j F_W^{-1}(\mathbf{p} + \mathbf{k}_1, p_0 + k_{10}) \Gamma_i]^{(a'')} [\Gamma_i F_W^{-1}(-\mathbf{p}' + \mathbf{k}_1, -p'_0 + k_{10}) \Gamma_j]^{(b'')} \} \\ \times [F_W^{(a)}(\mathbf{p}, p_0) F_W^{(b)}(-\mathbf{p}, -p_0)]^{-1} [k_1^2 - m_1^2 + i\delta]^{-1}. \quad (2.9)$$

Here m_1 and m_2 denote the two meson masses, and the Γ_i and Γ_j denote the nucleon-nucleon-meson vertices, which follow from the interaction Hamiltonians (see below). Because here we only consider nucleons in the intermediate state, we have $a = a' = a'' = N$ and $b = b' = b'' = N$. Note that the first term between the curly brackets corresponds to the planar-box two-meson-exchange diagram and the second term to the crossed-box two-meson-exchange diagram. In these diagrams only the contribution of the positive-energy nucleon states are included, in accordance with the pair-suppression hypothesis that we used in our earlier work on two-meson exchange [3–5].

The fourth-order potential $V^{(4)}$ consists of two parts. The first part is given by the fourth-order planar and crossed BW diagrams, shown in Figs. 1(a) and 1(b)–1(d), respectively, and their ‘‘mirror’’ counterparts. The second part is due to the fact that we do not distinguish the two different time orderings (i.e., the explicit energy dependence) in the one-boson-exchange diagrams. Hence, solving the scattering equation does not generate the time-ordered TMO diagrams of Figs. 2(a) and 2(b) nor their ‘‘mirror’’ counterparts. We therefore include these TMO diagrams explicitly [20], subtracting the once-iterated one-meson contribution

$$K_{\text{Born}}^{(4)} = K^{(2)} g K^{(2)} = V^{(2)} g V^{(2)}, \quad (2.10)$$

and so the fourth-order potential reads

$$V(\mathbf{p}', \mathbf{p}) = K^{(4)} - K^{(2)} g K^{(2)}. \quad (2.11)$$

The procedure to derive the kernels for the planar and crossed graphs corresponding to Figs. 1 and 2 is amply described in Refs. [4,5] and will not be repeated here. From the worked-out vertices (see below) and closely following the procedure as discussed in the referred papers, the contribution of the different graphs can be written down immediately. Finally, when the mesons are distinguishable, we also have to include the contributions from the diagrams where we interchange the two meson lines (dashed and dotted lines in Figs. 1 and 2). They merely give rise to a factor of 2 when we evaluate the potentials.

For point couplings the nucleon-nucleon-meson Hamiltonians are [21]

$$\mathcal{H}_{PV} = \frac{f_{PV}}{m_\pi} \bar{\psi} \gamma_5 \gamma_\mu \boldsymbol{\tau} \psi \cdot \partial^\mu \boldsymbol{\phi}_{PV}, \quad (2.12a)$$

$$\mathcal{H}_S = g_S \bar{\psi} \boldsymbol{\tau} \psi \cdot \boldsymbol{\phi}_S, \quad (2.12b)$$

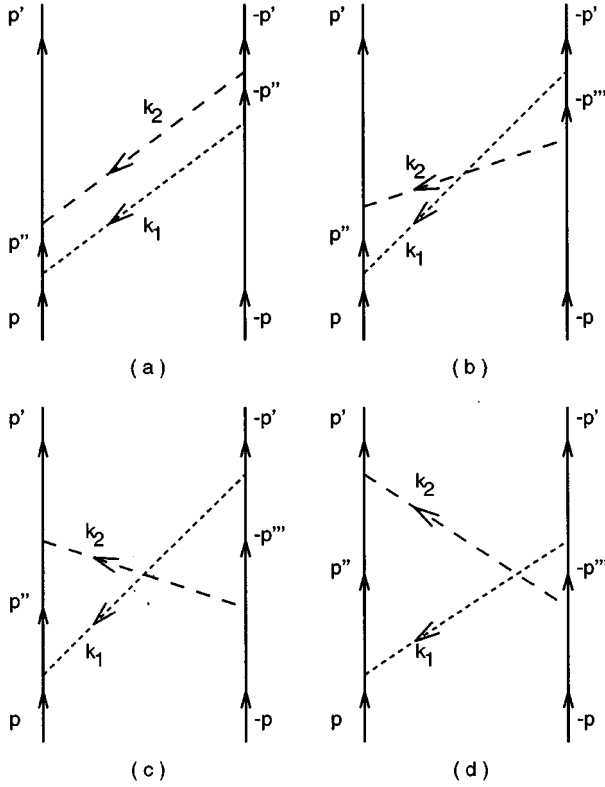


FIG. 1. BW two-meson-exchange graphs: (a) planar and (b)–(d) crossed box. The dotted line with momentum \mathbf{k}_1 refers to the pion and the dashed line with momentum \mathbf{k}_2 refers to one of the other (vector, scalar, or pseudoscalar) mesons. To these we have to add the “mirror” graphs, and the graphs where we interchange the two meson lines.

$$\mathcal{H}_V = g_V \bar{\psi} \gamma_\mu \boldsymbol{\tau} \psi \cdot \boldsymbol{\phi}_V^\mu - \frac{f_V}{2M} \bar{\psi} \sigma_{\mu\nu} \boldsymbol{\tau} \psi \cdot \partial^\nu \boldsymbol{\phi}_V^\mu, \quad (2.12c)$$

where $\boldsymbol{\phi}$ denotes the pseudoscalar-, scalar-, and vector-meson fields, respectively. For the isoscalar ($I=0$) mesons, the isospin Pauli matrices $\boldsymbol{\tau}$ are absent. The nucleon-nucleon-Pomeron vertex has the same Lorentz structure as the isoscalar scalar vertex.

As is well known, the pseudoscalar one-meson exchange can also be represented by the pseudoscalar interaction Hamiltonian

$$\mathcal{H}_{PS} = g_{PS} \bar{\psi} i \gamma_5 \boldsymbol{\tau} \psi \cdot \boldsymbol{\phi}_{PS}. \quad (2.13)$$

Both \mathcal{H}_{PV} and \mathcal{H}_{PS} give rise to the same on-energy-shell one-meson-exchange potential provided that the coupling constants satisfy the relation $f_{PV}/m_\pi = g_{PS}/2M$. From this we tacitly assume that the pseudovector coupling constant f_{PV} is $\mathcal{O}(1/M)$. This simplifies the expressions for the pion-pseudoscalar potentials considerably.

The generalization of the interaction kernels to the case with a Gaussian (or any other) form factor has been treated and explained in [3]. The same procedure can be applied to the various meson exchanges to be considered here. The form factors $F_\alpha(\mathbf{k}^2)$ and $F_\pi(\mathbf{k}^2)$, which describe the meson-exchange and π -exchange amplitudes, respectively, are

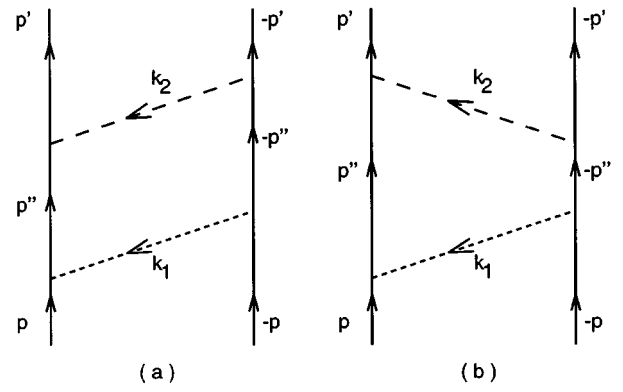


FIG. 2. Planar-box TMO two-meson-exchange graphs. Same notation as in Fig. 1. To these we have to add the “mirror” graphs, and the graphs where we interchange the two meson lines.

simply a product of the Gaussian vertex form factors $F_{NN\alpha}(\mathbf{k}^2) = \exp(-\mathbf{k}^2/2\Lambda_{NN\alpha}^2)$ and $F_{NN\pi}(\mathbf{k}^2) = \exp(-\mathbf{k}^2/2\Lambda_{NN\pi}^2)$.

III. DEFINITION OF THE NUCLEON-NUCLEON TME POTENTIAL

The transition from Dirac spinors to Pauli spinors is reviewed in Appendix C of Ref. [3]. There we derived the Lippmann-Schwinger equation

$$\chi(\mathbf{p}') = \chi^{(0)}(\mathbf{p}') + \tilde{g}(\mathbf{p}') \int d^3p \mathcal{V}(\mathbf{p}', \mathbf{p}) \chi(\mathbf{p}) \quad (3.1)$$

for the Pauli-spinor wave functions $\chi(\mathbf{p})$. The wave function $\chi(\mathbf{p})$ and the potential $\mathcal{V}(\mathbf{p}', \mathbf{p})$ in the Pauli-spinor space are defined by

$$\phi(\mathbf{p}) = \sum_{\sigma_a, \sigma_b} \chi_{\sigma_a \sigma_b}(\mathbf{p}) u_a(\mathbf{p}, \sigma_a) u_b(-\mathbf{p}, \sigma_b) \quad (3.2)$$

and

$$\begin{aligned} \chi_{\sigma'_a}^{(a)\dagger} \chi_{\sigma'_b}^{(b)\dagger} \mathcal{V} \chi_{\sigma_a}^{(a)} \chi_{\sigma_b}^{(b)} &= \bar{u}_a(\mathbf{p}', \sigma'_a) \bar{u}_b(-\mathbf{p}', \sigma'_b) V(\mathbf{p}', \mathbf{p}) \\ &\times u_a(\mathbf{p}, \sigma_a) u_b(-\mathbf{p}, \sigma_b). \end{aligned} \quad (3.3)$$

Like in the derivation of the OBE potentials [2,12], we make the approximation

$$E(\mathbf{p}) = (\mathbf{p}^2 + M^2)^{1/2} \approx M + \mathbf{p}^2/2M$$

everywhere in the interaction kernels of Sec. IV, which of course is fully justified for low energies only. We have a similar expansion for the on-shell energy,

$$W = 2(\mathbf{p}_i^2 + M^2)^{1/2} \approx 2M + \mathbf{p}_i^2/M.$$

In contrast to this kind of approximation, the full \mathbf{k}^2 dependence of the form factors is kept throughout the derivation of the two-meson-exchange potential. Note that the Gaussian form factors suppress the high-momentum transfers strongly. This means that the contribution to the potentials from intermediate states which are far off energy shell cannot be very

large. It also means that the $1/M$ expansions can be expected to be valid up to larger energies as well.

The reduction of the TME potential from Dirac-spinor

space to Pauli-spinor space is completely similar to the procedures discussed in Refs. [3–5]. The vertex operators in Pauli-spinor space up to order $1/M^2$ are given by

$$\bar{u}(\mathbf{p}')\Gamma_{PV}^{(a)}u(\mathbf{p}) = -i\left(\frac{f_{PV}}{m_\pi}\right)\left[\boldsymbol{\sigma}_1 \cdot \mathbf{k}\left(1 - \frac{\mathbf{p}'^2 + \mathbf{p}^2}{8M^2}\right) \pm \frac{\omega}{2M}\boldsymbol{\sigma}_1 \cdot (\mathbf{p}' + \mathbf{p}) + \frac{\mathbf{p}'^2 - \mathbf{p}^2}{8M^2}\boldsymbol{\sigma}_1 \cdot (\mathbf{p}' + \mathbf{p})\right], \quad (3.4)$$

$$\bar{u}(\mathbf{p}')\Gamma_{PS}^{(a)}u(\mathbf{p}) = -i\frac{g_{PS}}{2M}\left[\boldsymbol{\sigma}_1 \cdot \mathbf{k}\left(1 - \frac{\mathbf{p}'^2 + \mathbf{p}^2}{8M^2}\right) - \frac{\mathbf{p}'^2 - \mathbf{p}^2}{8M^2}\boldsymbol{\sigma}_1 \cdot (\mathbf{p}' + \mathbf{p})\right], \quad (3.5)$$

$$\bar{u}(\mathbf{p}')\Gamma_S^{(a)}u(\mathbf{p}) = g_S\left[1 - \frac{\mathbf{p}' \cdot \mathbf{p} + i\boldsymbol{\sigma}_1 \cdot \mathbf{p}' \times \mathbf{p}}{4M^2}\right], \quad (3.6)$$

$$\bar{u}(\mathbf{p}')\Gamma_V^{(a)}u(\mathbf{p}) = g_V\left[1 + \frac{\mathbf{p}' \cdot \mathbf{p} + i\boldsymbol{\sigma}_1 \cdot \mathbf{p}' \times \mathbf{p}}{4M^2} - \kappa_V \frac{(\mathbf{p}' - \mathbf{p})^2 - 2i\boldsymbol{\sigma}_1 \cdot \mathbf{p}' \times \mathbf{p}}{4M^2}\right]\phi_V^0 - \frac{g_V}{2M}[(\mathbf{p}' + \mathbf{p}) + i(1 + \kappa_V)\boldsymbol{\sigma}_1 \times \mathbf{k}] \cdot \boldsymbol{\phi}_V, \quad (3.7)$$

where $\mathbf{k} = \mathbf{p}' - \mathbf{p}$ and $\kappa_V = f_V/g_V$. The expressions for $\bar{u}(-\mathbf{p}')\Gamma^{(b)}u(-\mathbf{p})$ are trivially obtained by substituting $(\mathbf{p}', \mathbf{p}, \mathbf{k}, \boldsymbol{\sigma}_1) \rightarrow (-\mathbf{p}', -\mathbf{p}, -\mathbf{k}, \boldsymbol{\sigma}_2)$. For the isovector ($I=1$) mesons, the appropriate isospin matrices have to be attached. In the Γ -matrix element of Eq. (3.4), the upper sign applies to the creation and the lower sign to the absorption of the pseudoscalar meson at the vertex.

Although we will assume the pseudovector coupling for the pion, we here have also listed the vertex operator in the case of pseudoscalar coupling for reasons of completeness, which might be helpful for later work by other groups. The changes can be easily accounted for, as we will indicate in the following sections.

Useful for the evaluation of the second-order diagrams are the relations

$$\tau_j \tau_i = \delta_{ij} + i\epsilon_{jik}\tau_k, \quad \sigma_j \sigma_i = \delta_{ij} + i\epsilon_{jik}\sigma_k. \quad (3.8)$$

Products of this type will occur for each nucleon line. The isospin factors for the planar ($//$) and crossed (X) diagrams can readily be evaluated. In the case of two isospin-1 mesons, we have

$$\begin{aligned} C_{NN}^{(//)}(I) &= 3 - 2\boldsymbol{\tau}_1 \cdot \boldsymbol{\tau}_2, \\ C_{NN}^{(X)}(I) &= 3 + 2\boldsymbol{\tau}_1 \cdot \boldsymbol{\tau}_2, \end{aligned} \quad (3.9)$$

where I denotes the total isospin of the NN state. For the exchange of an isospin-1 with an isospin-0 exchange, one has

$$C_{NN}^{(//)}(I) = C_{NN}^{(X)}(I) \equiv C_{NN}^{(1,0)}(I) = \boldsymbol{\tau}_1 \cdot \boldsymbol{\tau}_2. \quad (3.10)$$

In order to obtain the contributions to the potentials in the adiabatic approximation, we expand the energy denominators in the expressions for the planar and the crossed-box diagrams and keep only the leading term. So, for example,

$$\frac{1}{E(\mathbf{p}) + E(\mathbf{p}') - W + \omega} \approx \frac{1}{\omega} \left[1 + \frac{\mathbf{k}_1 \cdot \mathbf{k}_2 - \mathbf{q} \cdot (\mathbf{k}_1 - \mathbf{k}_2)}{2M\omega} \right], \quad (3.11)$$

where we have made the on-energy-shell approximation $\mathbf{p}^2 - \mathbf{p}_i^2 = 0$ and $\mathbf{p}'^2 - \mathbf{p}_i^2 = 0$, with \mathbf{p}_i the initial-state momentum, and where we introduced $\mathbf{q} = \frac{1}{2}(\mathbf{p}' + \mathbf{p})$. The second term between square brackets gives the nonadiabatic contribution to the potentials, presented in Sec. V A. The term proportional to $\mathbf{q} \cdot (\mathbf{k}_1 - \mathbf{k}_2)$ usually drops out for symmetry reasons. The only exceptions occur for the planar-box nonadiabatic pion-pseudoscalar potentials (see Sec. V A).

In the following, we will concentrate on the derivation of the pion-meson potentials, which are expected to be the most important ones. The derivation of the more general case of two arbitrary mesons (not necessarily involving at least one pion) will then be straightforward.

IV. PION-MESON-EXCHANGE POTENTIALS

A. Pion-pseudoscalar exchange

Using the assumption that the pseudovector coupling constants are $\mathcal{O}(1/M)$ [see the discussion below Eq. (2.12a)], we can neglect all $1/M^2$ contributions and the pion-pseudoscalar-exchange potential is the simplest potential we will encounter. As a representative of the pseudoscalar mesons we select the η and derive the $\pi\eta$ -exchange potential.

TABLE I. Adiabatic approximation of the energy denominators $D_i(\omega_1, \omega_2)$ for the planar and crossed diagrams.

Planar ($//$)	$+ \frac{1}{2\omega_1\omega_2} \left[\frac{1}{\omega_1} + \frac{1}{\omega_2} - \frac{1}{(\omega_1 + \omega_2)} \right]$
Crossed (X)	$- \frac{1}{2\omega_1\omega_2} \left[\frac{1}{\omega_1} + \frac{1}{\omega_2} - \frac{1}{(\omega_1 + \omega_2)} \right]$

TABLE II. The momentum operators $O^{(i)}(\mathbf{k}_1, \mathbf{k}_2)$ for the planar ($//$) and crossed (X) π -meson-exchange diagrams. The subscripts PS and S refer to the π -pseudoscalar and π -scalar operators, respectively. The subscripts e and m refer to the electric and magnetic parts of the π -vector operators, and $\kappa = f_V/g_V$. The \mp sign refers to pseudovector or pseudoscalar coupling for the pion, respectively.

Type	$O^{(i)}(\mathbf{k}_1, \mathbf{k}_2)$
$O_{PS}^{(//)}$	$2(\mathbf{k}_1 \cdot \mathbf{k}_2)^2 - 2\boldsymbol{\sigma}_1 \cdot (\mathbf{k}_1 \times \mathbf{k}_2)\boldsymbol{\sigma}_2 \cdot (\mathbf{k}_1 \times \mathbf{k}_2)$
$O_{PS}^{(X)}$	$2(\mathbf{k}_1 \cdot \mathbf{k}_2)^2 + 2\boldsymbol{\sigma}_1 \cdot (\mathbf{k}_1 \times \mathbf{k}_2)\boldsymbol{\sigma}_2 \cdot (\mathbf{k}_1 \times \mathbf{k}_2)$
$O_S^{(//)}$	$\left[2 + \frac{\mathbf{k}_2^2 + \mathbf{k}_1 \cdot \mathbf{k}_2}{2M^2} - \frac{\mathbf{q}^2 + \frac{1}{4}\mathbf{k}^2}{M^2} \right] \boldsymbol{\sigma}_1 \cdot \mathbf{k}_1 \boldsymbol{\sigma}_2 \cdot \mathbf{k}_1$ $- \frac{1}{4M^2} [(\mathbf{k}_1^2 \mp \mathbf{k}_1 \cdot \mathbf{k}_2)(\boldsymbol{\sigma}_1 \cdot \mathbf{k}_1 \boldsymbol{\sigma}_2 \cdot \mathbf{k}_2 + \boldsymbol{\sigma}_1 \cdot \mathbf{k}_2 \boldsymbol{\sigma}_2 \cdot \mathbf{k}_1) + 2i\mathbf{q} \cdot (\mathbf{k}_1 \times \mathbf{k}_2)(\boldsymbol{\sigma}_1 + \boldsymbol{\sigma}_2) \cdot \mathbf{k}_1]$
$O_S^{(X)}$	$\left[2 + \frac{\mathbf{k}_2^2 + \mathbf{k}_1 \cdot \mathbf{k}_2}{2M^2} - \frac{\mathbf{q}^2 + \frac{1}{4}\mathbf{k}^2}{M^2} \right] \boldsymbol{\sigma}_1 \cdot \mathbf{k}_1 \boldsymbol{\sigma}_2 \cdot \mathbf{k}_1$ $- \frac{1}{4M^2} [(\mathbf{k}_1^2 \mp \mathbf{k}_1 \cdot \mathbf{k}_2)(\boldsymbol{\sigma}_1 \cdot \mathbf{k}_1 \boldsymbol{\sigma}_2 \cdot \mathbf{k}_2 + \boldsymbol{\sigma}_1 \cdot \mathbf{k}_2 \boldsymbol{\sigma}_2 \cdot \mathbf{k}_1) + 2i\mathbf{q} \cdot (\mathbf{k}_1 \times \mathbf{k}_2)(\boldsymbol{\sigma}_1 + \boldsymbol{\sigma}_2) \cdot \mathbf{k}_1]$
$O_{e,e}^{(//)}$	$\left[-2 - 3\frac{\mathbf{q}^2 + \frac{1}{4}\mathbf{k}^2}{M^2} + \frac{\mathbf{k}_1^2 + 4\mathbf{k}_1 \cdot \mathbf{k}_2 + \mathbf{k}_2^2}{2M^2} - \frac{\mathbf{k}_1^2}{2M^2} \right] \boldsymbol{\sigma}_1 \cdot \mathbf{k}_1 \boldsymbol{\sigma}_2 \cdot \mathbf{k}_1 \mp \frac{\mathbf{k}_1 \cdot \mathbf{k}_2}{4M^2} (\boldsymbol{\sigma}_1 \cdot \mathbf{k}_1 \boldsymbol{\sigma}_2 \cdot \mathbf{k}_2 + \boldsymbol{\sigma}_1 \cdot \mathbf{k}_2 \boldsymbol{\sigma}_2 \cdot \mathbf{k}_1)$
$O_{e,e}^{(X)}$	$\left[-2 - 3\frac{\mathbf{q}^2 + \frac{1}{4}\mathbf{k}^2}{M^2} + \frac{\mathbf{k}_1^2 + 4\mathbf{k}_1 \cdot \mathbf{k}_2 + \mathbf{k}_2^2}{2M^2} + \frac{\mathbf{k}_1^2}{2M^2} \right] \boldsymbol{\sigma}_1 \cdot \mathbf{k}_1 \boldsymbol{\sigma}_2 \cdot \mathbf{k}_1 \mp \frac{\mathbf{k}_1 \cdot \mathbf{k}_2}{4M^2} (\boldsymbol{\sigma}_1 \cdot \mathbf{k}_1 \boldsymbol{\sigma}_2 \cdot \mathbf{k}_2 + \boldsymbol{\sigma}_1 \cdot \mathbf{k}_2 \boldsymbol{\sigma}_2 \cdot \mathbf{k}_1)$
$O_{e,m}^{(//)}$	$(1 + \kappa)[-2i\mathbf{q} \cdot (\mathbf{k}_1 \times \mathbf{k}_2)(\boldsymbol{\sigma}_1 + \boldsymbol{\sigma}_2) \cdot \mathbf{k}_1 + 2\mathbf{k}_1 \cdot \mathbf{k}_2 \boldsymbol{\sigma}_1 \cdot \mathbf{k}_1 \boldsymbol{\sigma}_2 \cdot \mathbf{k}_1 - \mathbf{k}_1^2(\boldsymbol{\sigma}_1 \cdot \mathbf{k}_1 \boldsymbol{\sigma}_2 \cdot \mathbf{k}_2 + \boldsymbol{\sigma}_1 \cdot \mathbf{k}_2 \boldsymbol{\sigma}_2 \cdot \mathbf{k}_1)]$
$O_{e,m}^{(X)}$	$(1 + \kappa)[-2i\mathbf{q} \cdot (\mathbf{k}_1 \times \mathbf{k}_2)(\boldsymbol{\sigma}_1 + \boldsymbol{\sigma}_2) \cdot \mathbf{k}_1 - 2\mathbf{k}_1 \cdot \mathbf{k}_2 \boldsymbol{\sigma}_1 \cdot \mathbf{k}_1 \boldsymbol{\sigma}_2 \cdot \mathbf{k}_1 + \mathbf{k}_1^2(\boldsymbol{\sigma}_1 \cdot \mathbf{k}_1 \boldsymbol{\sigma}_2 \cdot \mathbf{k}_2 + \boldsymbol{\sigma}_1 \cdot \mathbf{k}_2 \boldsymbol{\sigma}_2 \cdot \mathbf{k}_1)]$
$O_{e,2m}^{(//)}$	$(1 + 2\kappa)[-i\mathbf{q} \cdot (\mathbf{k}_1 \times \mathbf{k}_2)(\boldsymbol{\sigma}_1 + \boldsymbol{\sigma}_2) \cdot \mathbf{k}_1 + (\mathbf{k}_2^2 + \mathbf{k}_1 \cdot \mathbf{k}_2)\boldsymbol{\sigma}_1 \cdot \mathbf{k}_1 \boldsymbol{\sigma}_2 \cdot \mathbf{k}_1 - \frac{1}{2}\mathbf{k}_1^2(\boldsymbol{\sigma}_1 \cdot \mathbf{k}_1 \boldsymbol{\sigma}_2 \cdot \mathbf{k}_2 + \boldsymbol{\sigma}_1 \cdot \mathbf{k}_2 \boldsymbol{\sigma}_2 \cdot \mathbf{k}_1)]$
$O_{e,2m}^{(X)}$	$(1 + 2\kappa)[-i\mathbf{q} \cdot (\mathbf{k}_1 \times \mathbf{k}_2)(\boldsymbol{\sigma}_1 + \boldsymbol{\sigma}_2) \cdot \mathbf{k}_1 + (\mathbf{k}_2^2 + \mathbf{k}_1 \cdot \mathbf{k}_2)\boldsymbol{\sigma}_1 \cdot \mathbf{k}_1 \boldsymbol{\sigma}_2 \cdot \mathbf{k}_1 - \frac{1}{2}\mathbf{k}_1^2(\boldsymbol{\sigma}_1 \cdot \mathbf{k}_1 \boldsymbol{\sigma}_2 \cdot \mathbf{k}_2 + \boldsymbol{\sigma}_1 \cdot \mathbf{k}_2 \boldsymbol{\sigma}_2 \cdot \mathbf{k}_1)]$
$O_{m,m}^{(//)}$	$(1 + \kappa)^2[\mathbf{k}_1^2 \mathbf{k}_2^2 - (\mathbf{k}_1 \cdot \mathbf{k}_2)^2 + \mathbf{k}_2^2 \boldsymbol{\sigma}_1 \cdot \mathbf{k}_1 \boldsymbol{\sigma}_2 \cdot \mathbf{k}_1 - \mathbf{k}_1^2 \mathbf{k}_2^2 \boldsymbol{\sigma}_1 \cdot \boldsymbol{\sigma}_2 + \boldsymbol{\sigma}_1 \cdot (\mathbf{k}_1 \times \mathbf{k}_2)\boldsymbol{\sigma}_2 \cdot (\mathbf{k}_1 \times \mathbf{k}_2)]$
$O_{m,m}^{(X)}$	$(1 + \kappa)^2[\mathbf{k}_1^2 \mathbf{k}_2^2 - (\mathbf{k}_1 \cdot \mathbf{k}_2)^2 - \mathbf{k}_2^2 \boldsymbol{\sigma}_1 \cdot \mathbf{k}_1 \boldsymbol{\sigma}_2 \cdot \mathbf{k}_1 + \mathbf{k}_1^2 \mathbf{k}_2^2 \boldsymbol{\sigma}_1 \cdot \boldsymbol{\sigma}_2 - \boldsymbol{\sigma}_1 \cdot (\mathbf{k}_1 \times \mathbf{k}_2)\boldsymbol{\sigma}_2 \cdot (\mathbf{k}_1 \times \mathbf{k}_2)]$

The $\pi\pi$ -exchange potential has already been discussed in Ref. [3]. The purely off-shell term proportional to $(\mathbf{p}'^2 - \mathbf{p}^2)$ in the pseudovector vertex (3.4) gives rise to a $1/M$ term in the TMO diagrams, rather than a $1/M^2$ term. We defer this contribution to the potential to Sec. V C. Similarly, the contribution due to the ω/M term will be discussed in Sec. V B.

We assign (\mathbf{k}_1, ω_1) to the π meson and (\mathbf{k}_2, ω_2) to the η meson. The planar BW graph of Fig. 1(a), the TMO graphs of Fig. 2, and their ‘‘mirror’’ counterparts give

$$V_{\pi\eta}^{(0)}(//) = C_{NN}^{(1,0)}(I) \left(\frac{f_{NN\eta}}{m_\pi} \right)^2 \left(\frac{f_{NN\pi}}{m_\pi} \right)^2 \int \int \frac{d^3 k_1 d^3 k_2}{(2\pi)^6}$$

$$\times e^{i(\mathbf{k}_1 + \mathbf{k}_2) \cdot \mathbf{r}} F_\pi(\mathbf{k}_1^2) F_\eta(\mathbf{k}_2^2)$$

$$\times [\mathbf{k}_1 \cdot \mathbf{k}_2 - i\boldsymbol{\sigma}_1 \cdot (\mathbf{k}_1 \times \mathbf{k}_2)]$$

$$\times [\mathbf{k}_1 \cdot \mathbf{k}_2 - i\boldsymbol{\sigma}_2 \cdot (\mathbf{k}_1 \times \mathbf{k}_2)] D_{//}(\omega_1, \omega_2), \quad (4.1)$$

and the crossed BW graphs of Figs. 1(b)–1(d) and their ‘‘mirror’’ graphs give

$$V_{\pi\eta}^{(0)}(X) = C_{NN}^{(1,0)}(I) \left(\frac{f_{NN\eta}}{m_\pi} \right)^2 \left(\frac{f_{NN\pi}}{m_\pi} \right)^2 \int \int \frac{d^3 k_1 d^3 k_2}{(2\pi)^6}$$

$$\times e^{i(\mathbf{k}_1 + \mathbf{k}_2) \cdot \mathbf{r}} F_\pi(\mathbf{k}_1^2) F_\eta(\mathbf{k}_2^2)$$

$$\times [\mathbf{k}_1 \cdot \mathbf{k}_2 - i\boldsymbol{\sigma}_1 \cdot (\mathbf{k}_1 \times \mathbf{k}_2)]$$

$$\times [\mathbf{k}_1 \cdot \mathbf{k}_2 + i\boldsymbol{\sigma}_2 \cdot (\mathbf{k}_1 \times \mathbf{k}_2)] D_X(\omega_1, \omega_2). \quad (4.2)$$

Here $F_\pi(\mathbf{k}_1^2) = F_{NN\pi}^2(\mathbf{k}_1^2)$ and $F_\eta(\mathbf{k}_2^2) = F_{NN\eta}^2(\mathbf{k}_2^2)$, and the energy denominators $D_i(\omega_1, \omega_2)$ are given in Table I. Choosing the pseudoscalar coupling (3.5) instead of the pseudovector coupling (3.4) will result in the same leading-order potential.

The full separation of the \mathbf{k}_1 and \mathbf{k}_2 dependence of the Fourier integrals can be achieved as shown in Ref. [3]. Using

the λ -integral representation, Eq. (B4) of [3], one can derive that

$$\frac{1}{\omega^3} = \frac{2}{\pi} \int_0^\infty \frac{d\lambda}{\lambda^2} \left[\frac{1}{\omega^2} - \frac{1}{\omega^2 + \lambda^2} \right] \quad (4.3)$$

and

$$\frac{1}{\omega_1^2 \omega_2^2} \frac{1}{\omega_1 + \omega_2} = \frac{2}{\pi} \int_0^\infty \frac{d\lambda}{\lambda^2} \left[\frac{1}{\omega_1^2} - \frac{1}{\omega_1^2 + \lambda^2} \right] \left[\frac{1}{\omega_2^2} - \frac{1}{\omega_2^2 + \lambda^2} \right]. \quad (4.4)$$

In performing the Fourier transform, the $1/\omega^2$ term gives rise to the basic function $I_2(m, r) = (m/4\pi) \phi_C^0(m, r)$, where [2,12]

$$\begin{aligned} \phi_C^0(m, r) &= e^{m^2/\Lambda^2} \left[e^{-mr} \operatorname{erfc} \left(\frac{m}{\Lambda} - \frac{\Lambda r}{2} \right) \right. \\ &\quad \left. - e^{mr} \operatorname{erfc} \left(\frac{m}{\Lambda} + \frac{\Lambda r}{2} \right) \right] \frac{1}{2mr}. \end{aligned}$$

Similarly, the $1/(\omega^2 + \lambda^2)$ term gives rise to the function

$$F_\alpha(\lambda, r) = e^{-\lambda^2/\Lambda^2} I_2(\sqrt{m_\alpha^2 + \lambda^2}, r). \quad (4.5)$$

Therefore, the typical coordinate-space function for the planar and crossed diagrams is of the form

$$\begin{aligned} B_{\alpha\beta}(r_1, r_2) &= \frac{2}{\pi} \int_0^\infty \frac{d\lambda}{\lambda^2} [I_2(m_\alpha, r_1) I_2(m_\beta, r_2) \\ &\quad - F_\alpha(\lambda, r_1) F_\beta(\lambda, r_2)]. \end{aligned} \quad (4.6)$$

Accordingly, we derive from Eqs. (4.1) and (4.2) the form

$$\begin{aligned} V_{\pi\eta}^{(0)} &= \sum_{i=//, X} C_{NN}^{(1,0)}(I) \left(\frac{f_{NN\eta}}{m_\pi} \right)^2 \left(\frac{f_{NN\pi}}{m_\pi} \right)^2 \\ &\quad \times \lim_{\mathbf{r}_1, \mathbf{r}_2 \rightarrow \mathbf{r}} O_{PS}^{(i)}(-i\nabla_1, -i\nabla_2) B_{NN\pi\eta}^{(i)}(r_1, r_2), \end{aligned} \quad (4.7)$$

where

$$B_{NN\pi\eta}^{(//)}(r_1, r_2) = -B_{NN\pi\eta}^{(X)}(r_1, r_2) = \frac{1}{2} B_{\pi\eta}(r_1, r_2), \quad (4.8)$$

and the operators $O_{PS}^{(i)}(\mathbf{k}_1, \mathbf{k}_2)$ are given in Table II. We should point out that these operators contain the contributions from *all* graphs, including the contributions where we interchanged the π and η lines. This gives an overcounting when the particles are identical, and so in case of $\pi\pi$ exchange these operators should be divided by 2.

B. Pion-scalar exchange

To be definite we select from the scalar mesons the $a_0(980)$ and derive the πa_0 -exchange potential. The $\pi\epsilon(760)$ - and $\pi f_0(975)$ -exchange potentials can simply be obtained by an appropriate change of the isospin structure. In the following, (\mathbf{k}_1, ω_1) refers to the π meson and (\mathbf{k}_2, ω_2) refers to the a_0 meson.

We will evaluate the potentials up to order $1/M^2$. Using the vertices of Eqs. (3.4) and (3.6), and including the normalization factors of the nucleon Dirac spinors in the intermediate two-nucleon state, which also contribute a factor of order $1/M^2$, we readily obtain the contributions to the NN potentials. After some rearrangement, the planar graphs give

$$\begin{aligned} V_{\pi a_0}^{(0)}(//) &= C_{NN}^{(//)}(I) g_{NNa_0}^2 \left(\frac{f_{NN\pi}}{m_\pi} \right)^2 \int \int \frac{d^3 k_1 d^3 k_2}{(2\pi)^6} e^{i(\mathbf{k}_1 + \mathbf{k}_2) \cdot \mathbf{r}} F_\pi(\mathbf{k}_1^2) F_{a_0}(\mathbf{k}_2^2) \\ &\quad \times \left\{ \left[1 - \frac{\mathbf{p}' \cdot \mathbf{p}'' + i\boldsymbol{\sigma}_1 \cdot \mathbf{p}' \times \mathbf{p}''}{4M^2} \right] \left[1 - \frac{\mathbf{p}' \cdot \mathbf{p}'' + i\boldsymbol{\sigma}_2 \cdot \mathbf{p}' \times \mathbf{p}''}{4M^2} \right] (\boldsymbol{\sigma}_1 \cdot \mathbf{k}_1) (\boldsymbol{\sigma}_2 \cdot \mathbf{k}_1) N_{//}(\mathbf{p}'') \right. \\ &\quad \left. + \frac{\mathbf{p}'^2 - \mathbf{p}^2}{8M^2} [\boldsymbol{\sigma}_1 \cdot \mathbf{k}_1 \boldsymbol{\sigma}_2 \cdot (\mathbf{p}' + \mathbf{p}) + \boldsymbol{\sigma}_1 \cdot (\mathbf{p}'' + \mathbf{p}) \boldsymbol{\sigma}_2 \cdot \mathbf{k}_1] \right\} D_{//}(\omega_1, \omega_2), \end{aligned} \quad (4.9)$$

and the crossed graphs give

$$\begin{aligned} V_{\pi a_0}^{(0)}(X) &= C_{NN}^{(X)}(I) g_{NNa_0}^2 \left(\frac{f_{NN\pi}}{m_\pi} \right)^2 \int \int \frac{d^3 k_1 d^3 k_2}{(2\pi)^6} e^{i(\mathbf{k}_1 + \mathbf{k}_2) \cdot \mathbf{r}} F_\pi(\mathbf{k}_1^2) F_{a_0}(\mathbf{k}_2^2) \\ &\quad \times \left\{ \left[1 - \frac{\mathbf{p}' \cdot \mathbf{p}'' + i\boldsymbol{\sigma}_1 \cdot \mathbf{p}' \times \mathbf{p}''}{4M^2} \right] (\boldsymbol{\sigma}_1 \cdot \mathbf{k}_1) (\boldsymbol{\sigma}_2 \cdot \mathbf{k}_1) \left[1 - \frac{\mathbf{p}''' \cdot \mathbf{p} + i\boldsymbol{\sigma}_2 \cdot \mathbf{p}''' \times \mathbf{p}}{4M^2} \right] N_X(\mathbf{p}'', \mathbf{p}''') \right. \\ &\quad \left. + \frac{\mathbf{p}'^2 - \mathbf{p}^2}{8M^2} \boldsymbol{\sigma}_1 \cdot \mathbf{k}_1 \boldsymbol{\sigma}_2 \cdot (\mathbf{p}' + \mathbf{p}''') + \frac{\mathbf{p}''^2 - \mathbf{p}^2}{8M^2} \boldsymbol{\sigma}_1 \cdot (\mathbf{p}'' + \mathbf{p}) \boldsymbol{\sigma}_2 \cdot \mathbf{k}_1 \right\} D_X(\omega_1, \omega_2). \end{aligned} \quad (4.10)$$

Here we introduced momentum vectors for the intermediate nucleon lines, given by

$$\begin{aligned}\mathbf{p}'' &= \mathbf{p} + \mathbf{k}_1 = \mathbf{p}' - \mathbf{k}_2, \\ \mathbf{p}''' &= \mathbf{p} + \mathbf{k}_2 = \mathbf{p}' - \mathbf{k}_1,\end{aligned}\quad (4.11)$$

and the functions

$$\begin{aligned}N_{//}(\mathbf{p}'') &= 1 + \frac{\mathbf{p}''^2 - \mathbf{p}^2}{4M^2}, \\ N_X(\mathbf{p}'', \mathbf{p}''') &= 1 + \frac{\mathbf{p}''^2 - \mathbf{p}^2}{8M^2} + \frac{\mathbf{p}'''^2 - \mathbf{p}'^2}{8M^2}.\end{aligned}\quad (4.12)$$

Again, the energy denominators $D_i(\omega_1, \omega_2)$ are given in Table I, and for all graphs $F_\pi(\mathbf{k}_1^2) = F_{NN\pi}^2(\mathbf{k}_1^2)$ and $F_{a_0}(\mathbf{k}_2^2) = F_{NNa_0}^2(\mathbf{k}_2^2)$. Including the ‘‘time-reversed’’ diagrams, the resulting coordinate-space potential can be written in the form

$$\begin{aligned}V_{\pi a_0}^{(0)} &= \sum_{i=//, X} C_{NN}^{(i)}(I) g_{NNa_0}^2 \left(\frac{f_{NN\pi}}{m_\pi} \right)^2 \\ &\times \lim_{\mathbf{r}_1, \mathbf{r}_2 \rightarrow \mathbf{r}} O_S^{(i)}(-i\nabla_1, -i\nabla_2) B_{NN\pi a_0}^{(i)}(r_1, r_2),\end{aligned}\quad (4.13)$$

where $B_{NN\pi a_0}^{(i)}(r_1, r_2)$ is defined by Eq. (4.8). The operators $O_S^{(i)}(\mathbf{k}_1, \mathbf{k}_2)$ can be found in Table II. They contain the contributions from *all* graphs. The choice of pseudoscalar coupling (2.13) for the pion instead of pseudovector coupling (2.12a) results in a change of sign in one of the terms, as indicated in Table II.

The purely off-shell contribution proportional to $(\mathbf{p}''^2 - \mathbf{p}^2)$ gives rise to a $1/M$ term in the TMO diagrams, which will be discussed in Sec. V C. Similarly, the contribution due to the ω/M term in the pion vertex (3.4) will be discussed separately in Sec. V B.

Note that, up to this order, both planar and crossed diagrams give rise to the same momentum operators $O_S(\mathbf{k}_1, \mathbf{k}_2)$. As a consequence, the planar and crossed contributions for the $\pi\varepsilon$ and πf_0 potentials exactly cancel, and hence

$$V_{\pi\varepsilon}^{(0)} = V_{\pi f_0}^{(0)} = 0. \quad (4.14)$$

C. Pion-Pomeron exchange

The pion-Pomeron potential has the same structure as the pion-scalar potential, except for an overall minus sign. Hence,

$$V_{\pi P}^{(0)} = 0. \quad (4.15)$$

Although the leading-order part of the potential vanishes, the $1/M$ corrections to the potential do not, and so in order to be able to evaluate the pion-Pomeron potentials in coordinate space, it is appropriate here first to point out the peculiarities of Pomeron exchange with respect to meson exchange. We use as a working hypothesis that there is a contribution to the

potential which corresponds to the Pomeron phenomenon at high energies. In QCD, the physical nature of Pomeron exchange is understood as color-singlet two- or multiple-gluon exchange [22–24]. The assumption that the Pomeron for our purposes can be described effectively by a simple Regge pole is part of our phenomenological and practical approach. In the Nijmegen OBE models Pomeron exchange provides a significant contribution to the short-range repulsion. We refer the interested reader to Refs. [2,12,25], and references cited therein. It remains to be seen whether Pomeron exchange, using some plausible form for it, is still a useful concept when we include many more contributions (i.e., two-meson contributions) than were taken into account in the Nijmegen OBE models. But the inclusion of the potentials involving the Pomeron is important in order to have the full consequences of the Pomeron worked out. Hence, at this stage these potentials are important for an extension of the Nijmegen OBE model.

We treat the Pomeron as a Regge pole, using the Durand–van Hove model [26]. Accordingly, in dealing with Pomeron exchange, we replace the OBE factor for meson exchange by an infinite sum over all even J , i.e.,

$$\frac{g^2}{m^2 - t} \Rightarrow A_P(t) = \sum_{J \text{ even}} (2J+1) \frac{g^2(J)}{\omega_J^2(t)}, \quad (4.16)$$

where

$$\omega_J^2(t) = m_J^2 - t \approx \mathbf{k}^2 + m_J^2. \quad (4.17)$$

Following the same procedure as in the OBE model [25] (i.e., the Khuri-Jones procedure for a Regge pole), and using the Sommerfeld-Watson transform, one gets for the Durand–van Hove sum in Eq. (4.16) the expression

$$\begin{aligned}A_P(t) &= \sum_{J \text{ even}} (2J+1) A_J(t), \\ A_J(t) &= -\beta(t) \frac{e^{-[J-\alpha(t)]\xi}}{\alpha(t) - J}.\end{aligned}\quad (4.18)$$

Here $\alpha(t)$ is the solution of the equation $m_J^2 - t = 0$, $\beta(t)$ is the residue at the pole, and ξ is a parameter in the Khuri-Jones representation (see [25]). For low energies, our region of interest here, ξ is such that one can restrict oneself to the lowest J value in Eq. (4.18), which is $J=0$. However, we should point out that in the case of the Pomeron the $J=0$ contribution from the Khuri-Jones procedure has nothing to do with a physical particle. With the Chew ghost-killing factor, $\beta(t) = -\alpha(t)\exp(\alpha\rho t)$, one obtains for Pomeron exchange at low energies from Eq. (4.18) the representation [25]

$$A_P(t) = \frac{g_P^2}{M^2} \exp\left(\frac{t}{4m_P^2}\right), \quad (4.19)$$

where the Pomeron-nucleon-nucleon coupling and the effective Pomeron mass can be expressed as [25]

$$g_P^2 = \gamma_P(0)(\bar{s}_R/M^2)^{\alpha_P(0)},$$

$$m_P^2 = \frac{1}{4} \left[a_P + \alpha'_P \ln \frac{\bar{s}_R}{M^2} \right]^{-1}. \quad (4.20)$$

With this preparation, we can now explain the treatment of the pion-Pomeron contribution to the potentials. As we will see in the next section, for the Pomeron contributions we encounter in the energy denominators the factors $1/\omega_J^2$ and $1/\omega_J^4$. The handling of the first term is discussed above and that of the second is easily inferred by observing that

$$A_4(t) = \sum_{J \text{ even}} (2J+1) \frac{g^2(J)}{\omega_J^4(t)} = \frac{d}{dt} A_P(t). \quad (4.21)$$

From Eq. (4.19) we therefore find that

$$A_4(t) = \frac{1}{4m_P^2} A_P(t). \quad (4.22)$$

The result of this analysis is that the basic Pomeron functions are

$$I_2(m, r) \rightarrow I_G(m_P, r),$$

$$I_4(m, r) \rightarrow \frac{1}{4m_P^2} I_G(m_P, r), \quad (4.23)$$

where

$$I_G(m_P, r) = \frac{m_P}{4\pi} \frac{4}{\sqrt{\pi}} \left(\frac{m_P}{M} \right)^2 e^{-m_P^2 r^2}. \quad (4.24)$$

With the substitutions (4.23), the treatment of the Pomeron is now completely analogous to that of the mesons.

D. Pion-vector exchange

As a result of the complexity of the vector-meson vertices (3.7), it is not very illuminating to give the various intermediate steps in the evaluation of the pion-vector-exchange potential. It suffices to note that it is convenient to separate the potential into four parts proportional to 1, $(1 + \kappa_V)$, $(1 + 2\kappa_V)$, and $(1 + \kappa_V)^2$, respectively. We refer to these as the electric-electric (e, e), the two electric-magnetic (e, m) and ($e, 2m$), and the magnetic-magnetic (m, m) terms. Assigning again (\mathbf{k}_1, ω_1) to the π meson and (\mathbf{k}_2, ω_2) to the ρ meson, we can then write the resulting potential as

$$V_{\pi\rho}^{(0)} = \sum_{i=//,X} C_{NN}^{(i)}(I) g_{NN\rho}^2 \left(\frac{f_{NN\pi}}{m_\pi} \right)^2 \int \int \frac{d^3 k_1 d^3 k_2}{(2\pi)^6}$$

$$\times e^{i(\mathbf{k}_1 + \mathbf{k}_2) \cdot \mathbf{r}} F_\pi(\mathbf{k}_1^2) F_\rho(\mathbf{k}_2^2)$$

$$\times \left[\frac{1}{2M^2} \{ O_{e,m}^{(i)} + O_{e,2m}^{(i)} + O_{m,m}^{(i)} \}(\mathbf{k}_1, \mathbf{k}_2) \right.$$

$$\left. + O_{e,e}^{(i)}(\mathbf{k}_1, \mathbf{k}_2) \right] D_i(\omega_1, \omega_2), \quad (4.25)$$

where the operators $O^{(i)}(\mathbf{k}_1, \mathbf{k}_2)$ can be found in Table II. They contain the contributions from *all* graphs. Again, the

TABLE III. Energy denominators $D_i^{(1)}(\omega_1, \omega_2)$ for the nonadiabatic corrections to the planar and crossed diagrams.

Planar (//)	$+\frac{1}{2\omega_1^2\omega_2^2} \left[\frac{1}{\omega_1^2} + \frac{1}{\omega_2^2} \right]$
Crossed (X)	$-\frac{1}{\omega_1^2\omega_2^2} \left[\frac{1}{\omega_1^2} + \frac{1}{\omega_2^2} \right]$

choice of pseudoscalar coupling for the pion instead of pseudovector coupling involves a simple change of sign in one of the terms in $O_{e,e}^{(i)}$.

The coordinate-space potential reads

$$V_{\pi\rho}^{(0)} = \sum_{i=//,X} C_{NN}^{(i)}(I) g_{NN\rho}^2 \left(\frac{f_{NN\pi}}{m_\pi} \right)^2$$

$$\times \lim_{\mathbf{r}_1, \mathbf{r}_2 \rightarrow \mathbf{r}} \left[\frac{1}{2M^2} \{ O_{e,m}^{(i)} + O_{e,2m}^{(i)} + O_{m,m}^{(i)} \} (-i\nabla_1, -i\nabla_2) \right.$$

$$\left. + O_{e,e}^{(i)}(-i\nabla_1, -i\nabla_2) \right] B_{NN\rho}^{(i)}(r_1, r_2). \quad (4.26)$$

The $\pi\omega$ and $\pi\phi$ potentials are again obtained by an appropriate change of the isospin structure. Note that in leading order (no $1/M^2$ contributions) the planar and crossed-box contributions exactly cancel for both $\pi\omega$ and $\pi\phi$ potentials; see Eq. (B8).

V. $1/M$ CORRECTIONS

A. Nonadiabatic corrections

The nonadiabatic correction from the $1/M$ expansion of the energy denominators is explained in Ref. [3]. The expansion of the energy denominators involves a momentum dependence which for all cases can be rewritten in the form $[\mathbf{k}_1 \cdot \mathbf{k}_2 \pm \mathbf{q} \cdot (\mathbf{k}_1 - \mathbf{k}_2)]/2M$. Separating off the momentum dependence, the energy denominators of Table I give rise to the nonadiabatic energy denominators $D_i^{(1)}$ as listed in Table III. Note that $D_X^{(1)} = -2D_{//}^{(1)}$, and so now the contributions from the planar and crossed diagrams for $\pi\epsilon(760)$, $\pi f_0(975)$, and πP do not cancel. We should point out that this expansion is only approximately valid, and in principle breaks down at the pion-production threshold ($T_{\text{lab}} \approx 280$ MeV).

In the crossed-box diagrams the \mathbf{q} dependence always cancels. Similarly, for pion-vector and pion-scalar (pion-Pomeron) exchange, the interchange of the two meson lines also removes the \mathbf{q} dependence. Hence, for pion-scalar exchange we get

$$V_{\pi\epsilon}^{(1a)}(i) = C_{NN}^{(1,0)}(I) g_{NN\epsilon}^2 \left(\frac{f_{NN\pi}}{m_\pi} \right)^2 \left(\frac{1}{M} \right)$$

$$\times \int \int \frac{d^3 k_1 d^3 k_2}{(2\pi)^6} e^{i(\mathbf{k}_1 + \mathbf{k}_2) \cdot \mathbf{r}} F_\pi(\mathbf{k}_1^2) F_\epsilon(\mathbf{k}_2^2) (\mathbf{k}_1 \cdot \mathbf{k}_2)$$

$$\times (\boldsymbol{\sigma}_1 \cdot \mathbf{k}_1) (\boldsymbol{\sigma}_2 \cdot \mathbf{k}_1) D_i^{(1)}(\omega_1, \omega_2), \quad (5.1)$$

where we took the $\pi\varepsilon$ potential as a particular example. Obviously, for pion-Pomeron exchange we get the same expression as for pion-scalar exchange, except for an overall minus sign. For pion-vector exchange we get

$$V_{\pi\rho}^{(1a)}(i) = -C_{NN}^{(i)}(I)g_{NN\rho}^2 \left(\frac{f_{NN\pi}}{m_\pi}\right)^2 \left(\frac{1}{M}\right) \int \int \frac{d^3k_1 d^3k_2}{(2\pi)^6} e^{i(\mathbf{k}_1+\mathbf{k}_2)\cdot\mathbf{r}} F_\pi(\mathbf{k}_1^2) F_\rho(\mathbf{k}_2^2) (\boldsymbol{\sigma}_1\cdot\mathbf{k}_1)(\boldsymbol{\sigma}_2\cdot\mathbf{k}_1) D_i^{(1)}(\omega_1, \omega_2), \quad (5.2)$$

where we took the $\pi\rho$ potential as a particular example and only kept the leading term in $O_{e,e}^{(i)}(\mathbf{k}_1, \mathbf{k}_2)$.

The situation for pion-pseudoscalar exchange is more subtle. As mentioned above, in the crossed-box diagrams the \mathbf{q} dependence cancels, resulting in

$$V_{\pi\eta}^{(1a)}(X) = C_{NN}^{(1,0)}(I) \left(\frac{f_{NN\eta}}{m_\pi}\right)^2 \left(\frac{f_{NN\pi}}{m_\pi}\right)^2 \left(\frac{1}{M}\right) \int \int \frac{d^3k_1 d^3k_2}{(2\pi)^6} e^{i(\mathbf{k}_1+\mathbf{k}_2)\cdot\mathbf{r}} F_\pi(\mathbf{k}_1^2) F_\eta(\mathbf{k}_2^2) (\mathbf{k}_1\cdot\mathbf{k}_2) \times [(\mathbf{k}_1\cdot\mathbf{k}_2)^2 + \boldsymbol{\sigma}_1\cdot(\mathbf{k}_1\times\mathbf{k}_2)\boldsymbol{\sigma}_2\cdot(\mathbf{k}_1\times\mathbf{k}_2)] D_X^{(1)}(\omega_1, \omega_2), \quad (5.3)$$

where we took the $\pi\eta$ potential as a particular example. In the planar-box diagram, on the other hand, the \mathbf{q} dependence survives and, after rearranging, we are left with

$$V_{\pi\eta}^{(1a)}(//) = C_{NN}^{(1,0)}(I) \left(\frac{f_{NN\eta}}{m_\pi}\right)^2 \left(\frac{f_{NN\pi}}{m_\pi}\right)^2 \left(\frac{1}{M}\right) \int \int \frac{d^3k_1 d^3k_2}{(2\pi)^6} e^{i(\mathbf{k}_1+\mathbf{k}_2)\cdot\mathbf{r}} F_\pi(\mathbf{k}_1^2) F_\eta(\mathbf{k}_2^2) (\mathbf{k}_1\cdot\mathbf{k}_2) \times [(\mathbf{k}_1\cdot\mathbf{k}_2)^2 - \boldsymbol{\sigma}_1\cdot(\mathbf{k}_1\times\mathbf{k}_2)\boldsymbol{\sigma}_2\cdot(\mathbf{k}_1\times\mathbf{k}_2) + i(\boldsymbol{\sigma}_1+\boldsymbol{\sigma}_2)\cdot(\mathbf{k}_1\times\mathbf{k}_2)\mathbf{q}\cdot(\mathbf{k}_1-\mathbf{k}_2)] D_{//}^{(1)}(\omega_1, \omega_2). \quad (5.4)$$

All integrals in Eqs. (5.1)–(5.4) can be readily evaluated using the results of Appendix A. Inspection of the energy denominators $D_i^{(1)}(\omega_1, \omega_2)$ reveals that we need derivatives of the function $I_4(m, r)$, which is defined by [3]

$$I_4(m, r) = -\frac{d}{dm^2} I_2(m, r) + \frac{1}{\Lambda^2} I_2(m, r), \quad (5.5)$$

while $I_4(m_\rho, r)$ for the Pomeron is given by the second expression in Eq. (4.23).

B. Pseudovector-vertex corrections

The pseudovector vertex gives rise to $1/M$ terms as shown in Eq. (3.4). In the planar-box diagrams, the $1/M$ contribution from each diagram is canceled by the $1/M$ contribution from its ‘‘mirror’’ diagram, and therefore we only have to consider the crossed-box BW diagrams. The pseudovector-vertex corrections are very simple to derive for the pion-scalar and pion-vector potentials. Below, we again take a representative meson for each type. Because of their simplicity, we also give the explicit coordinate-space expressions for these potentials. For pion-scalar exchange we get

$$V_{\pi\varepsilon}^{(1b)} = C_{NN}^{(1,0)}(I)g_{NN\varepsilon}^2 \left(\frac{f_{NN\pi}}{m_\pi}\right)^2 \left(\frac{1}{M}\right) \int \int \frac{d^3k_1 d^3k_2}{(2\pi)^6} e^{i(\mathbf{k}_1+\mathbf{k}_2)\cdot\mathbf{r}} F_\pi(\mathbf{k}_1^2) F_\varepsilon(\mathbf{k}_2^2) [(\boldsymbol{\sigma}_1\cdot\mathbf{k}_1)(\boldsymbol{\sigma}_2\cdot\mathbf{k}_2) + (\boldsymbol{\sigma}_1\cdot\mathbf{k}_2)(\boldsymbol{\sigma}_2\cdot\mathbf{k}_1)] \frac{1}{2\omega_1^2\omega_2^2} \\ = -C_{NN}^{(1,0)}(I)g_{NN\varepsilon}^2 \left(\frac{f_{NN\pi}}{m_\pi}\right)^2 \left(\frac{1}{3M}\right) I_2'(m_\pi, r) I_2'(m_\varepsilon, r) [(\boldsymbol{\sigma}_1\cdot\boldsymbol{\sigma}_2) + S_{12}]. \quad (5.6)$$

For pion-vector exchange we get

$$V_{\pi\rho}^{(1b)} = -C_{NN}^{(X)}(I)g_{NN\rho}^2 \left(\frac{f_{NN\pi}}{m_\pi}\right)^2 \left(\frac{1}{M}\right) \int \int \frac{d^3k_1 d^3k_2}{(2\pi)^6} e^{i(\mathbf{k}_1+\mathbf{k}_2)\cdot\mathbf{r}} F_\pi(\mathbf{k}_1^2) F_\rho(\mathbf{k}_2^2) [(\boldsymbol{\sigma}_1\cdot\mathbf{k}_1)(\boldsymbol{\sigma}_2\cdot\mathbf{k}_2) + (\boldsymbol{\sigma}_1\cdot\mathbf{k}_2)(\boldsymbol{\sigma}_2\cdot\mathbf{k}_1)] \frac{1}{2\omega_1^2\omega_2^2} \\ = C_{NN}^{(X)}(I)g_{NN\rho}^2 \left(\frac{f_{NN\pi}}{m_\pi}\right)^2 \left(\frac{1}{3M}\right) I_2'(m_\pi, r) I_2'(m_\rho, r) [(\boldsymbol{\sigma}_1\cdot\boldsymbol{\sigma}_2) + S_{12}]. \quad (5.7)$$

The pion-pseudoscalar case is more complicated than the pion-scalar and pion-vector cases, because now we also have to include the $1/M$ corrections from the pseudovector vertex of the η or η' meson. Again, the contributions from the planar-box diagrams are canceled by their ‘‘mirror’’ diagrams. Including the ‘‘time-reversed’’ diagrams, and defining the function

$$I_0(\Lambda, r) = \frac{1}{4\pi} \frac{\Lambda^3}{2\sqrt{\pi}} e^{-\Lambda^2 r^2/4}, \quad (5.8)$$

we find, for the crossed diagrams,

$$\begin{aligned}
V_{\pi\eta}^{(1b)} &= C_{NN}^{(1,0)}(I) \left(\frac{f_{NN\eta}}{m_\pi} \right)^2 \left(\frac{f_{NN\pi}}{m_\pi} \right)^2 \left(\frac{1}{M} \right) \int \int \frac{d^3k_1 d^3k_2}{(2\pi)^6} e^{i(\mathbf{k}_1+\mathbf{k}_2)\cdot\mathbf{r}} F_\pi(\mathbf{k}_1^2) F_\eta(\mathbf{k}_2^2) \\
&\quad \times \{ (\mathbf{k}_1 \cdot \mathbf{k}_2)(\mathbf{k}_1^2 + \mathbf{k}_2^2) + i(\boldsymbol{\sigma}_1 + \boldsymbol{\sigma}_2) \cdot [\mathbf{q} \times (\mathbf{k}_1 + \mathbf{k}_2)(\mathbf{k}_1 \cdot \mathbf{k}_2) + (\mathbf{k}_1 \times \mathbf{k}_2)\mathbf{q} \cdot (\mathbf{k}_1 - \mathbf{k}_2)] \} \frac{1}{\omega_1^2 \omega_2^2} \\
&= C_{NN}^{(1,0)}(I) \left(\frac{f_{NN\eta}}{m_\pi} \right)^2 \left(\frac{f_{NN\pi}}{m_\pi} \right)^2 \left(\frac{1}{M} \right) \left\{ [(m_\pi^2 + m_\eta^2) I_2'(m_\pi, r) I_2'(m_\eta, r) - I_0'(\Lambda_\pi, r) I_2'(m_\eta, r) - I_2'(m_\pi, r) I_0'(\Lambda_\eta, r)] \right. \\
&\quad \left. + \left[\frac{2}{r} [I_2''(m_\pi, r) I_2'(m_\eta, r) + I_2'(m_\pi, r) I_2''(m_\eta, r)] + \frac{4}{r^2} I_2'(m_\pi, r) I_2'(m_\eta, r) \right] \mathbf{L} \cdot \mathbf{S} \right\}. \tag{5.9}
\end{aligned}$$

C. Off-shell corrections in TMO diagrams

Next to the type of nonadiabatic (off-shell) corrections discussed in Sec. V A, there are $1/M$ corrections in the TMO diagrams, due to off-shell factors like $(\mathbf{p}''^2 - \mathbf{p}^2)$ from the pseudovector vertices [see Eq. (3.4)]. In the on-shell approximation $\mathbf{p}'^2 - \mathbf{p}_i^2 = \mathbf{p}^2 - \mathbf{p}_i^2 = 0$, this type of momentum dependence in the numerator cancels the $\mathbf{p}''^2 - \mathbf{p}_i^2$ momentum dependence of the two-nucleon intermediate state in the energy denominator of the TMO diagrams, leaving a $1/M$ correction to the potential.

For the pion-scalar and pion-vector exchanges it can be easily shown that these (what we call) off-shell TMO contributions involve the momentum operator

$$\begin{aligned}
O_{\text{off}}(\mathbf{k}_1, \mathbf{k}_2) &= \frac{1}{M} \left[\boldsymbol{\sigma}_1 \cdot \mathbf{k}_1 \boldsymbol{\sigma}_2 \cdot \mathbf{k}_1 \right. \\
&\quad \left. \mp \frac{1}{2} (\boldsymbol{\sigma}_1 \cdot \mathbf{k}_1 \boldsymbol{\sigma}_2 \cdot \mathbf{k}_2 + \boldsymbol{\sigma}_1 \cdot \mathbf{k}_2 \boldsymbol{\sigma}_2 \cdot \mathbf{k}_1) \right], \tag{5.10}
\end{aligned}$$

where the \mp sign refers to pseudovector or pseudoscalar coupling for the pion, respectively. Hence

$$\begin{aligned}
V_{\pi\varepsilon}^{(1c)} &= -C_{NN}^{(1,0)}(I) g_{NN\varepsilon}^2 \left(\frac{f_{NN\pi}}{m_\pi} \right)^2 \left(\frac{1}{2M} \right) F_\pi(\mathbf{k}_1^2) F_\varepsilon(\mathbf{k}_2^2) \\
&\quad \times O_{\text{off}}(\mathbf{k}_1, \mathbf{k}_2) \frac{1}{\omega_1^2 \omega_2^2}, \tag{5.11}
\end{aligned}$$

$$\begin{aligned}
V_{\pi\rho}^{(1c)} &= C_{NN}^{(1,0)}(I) g_{NN\rho}^2 \left(\frac{f_{NN\pi}}{m_\pi} \right)^2 \left(\frac{1}{2M} \right) F_\pi(\mathbf{k}_1^2) F_\rho(\mathbf{k}_2^2) \\
&\quad \times O_{\text{off}}(\mathbf{k}_1, \mathbf{k}_2) \frac{1}{\omega_1^2 \omega_2^2}. \tag{5.12}
\end{aligned}$$

Because the off-shell factors in the pseudovector vertices occur with the same $(\boldsymbol{\sigma}_1, \boldsymbol{\sigma}_2)$ spin dependence as the ω/M terms, it should be obvious that the resulting potentials are very similar to the pseudovector-vertex corrections derived in the previous section (except for a relative minus sign in the spin-orbit pion-pseudoscalar part). We find

$$\begin{aligned}
V_{\pi\eta}^{(1c)} &= C_{NN}^{(1,0)}(I) \left(\frac{f_{NN\eta}}{m_\pi} \right)^2 \left(\frac{f_{NN\pi}}{m_\pi} \right)^2 \left(\frac{1}{2M} \right) \\
&\quad \times \left\{ [(m_\pi^2 + m_\eta^2) I_2'_{2,\pi} I_2'_{2,\eta} - I_0'_{0,\pi} I_2'_{2,\eta} - I_2'_{2,\pi} I_0'_{0,\eta}] \right. \\
&\quad \left. + \left[\frac{2}{r} (I_2''_{2,\pi} I_2'_{2,\eta} + I_2'_{2,\pi} I_2''_{2,\eta}) - \frac{4}{r^2} I_2'_{2,\pi} I_2'_{2,\eta} \right] \mathbf{L} \cdot \mathbf{S} \right\}. \tag{5.13}
\end{aligned}$$

VI. RESULTS AND DISCUSSION

The complete pion-meson-exchange potential can be written as a sum of all pion-meson exchanges $V(\pi\alpha)$, where

$$V(\pi\alpha) = \sum_{n=0,1a,1b,1c} [V_{\pi\alpha}^{(n)}(//) + V_{\pi\alpha}^{(n)}(X)]. \tag{6.1}$$

Here, the second meson is denoted by α . Each potential consists of central, spin-spin, tensor, and spin-orbit parts. The leading-order contributions to the coordinate-space pion-meson potentials are given explicitly in Appendix B. The nonadiabatic $1/M$ corrections can be easily derived from Sec. V A and Appendix A, the pseudovector $1/M$ corrections are given in Sec. V B, and the extra $1/M$ corrections in the TMO diagrams are given in Sec. V C.

In the following we show the various contributions to the potentials, using the meson-nucleon coupling constants and cutoff masses as given in Table IV. They correspond to the

TABLE IV. Meson parameters employed in the potentials shown in Figs. 3–8. Coupling constants are at $\mathbf{k}^2=0$.

Meson	Mass (MeV)	$g/\sqrt{4\pi}$	$f/\sqrt{4\pi}$	$\kappa=f/g$	Λ (MeV)
π	138.04		0.269		853.9
η	547.45		0.124		950.0
η'	957.75		0.124		950.0
ρ	768.10	0.622	2.306	3.71	886.2
ω	781.95	3.336	-0.206	-0.06	1013.1
ϕ	1019.41	-1.202	0.078	-0.07	1013.1
a_0	982.70	1.847			679.4
ε	760.00	0.582			759.0
f_0	974.10	-2.372			759.0
Pomeron	309.10	1.884			

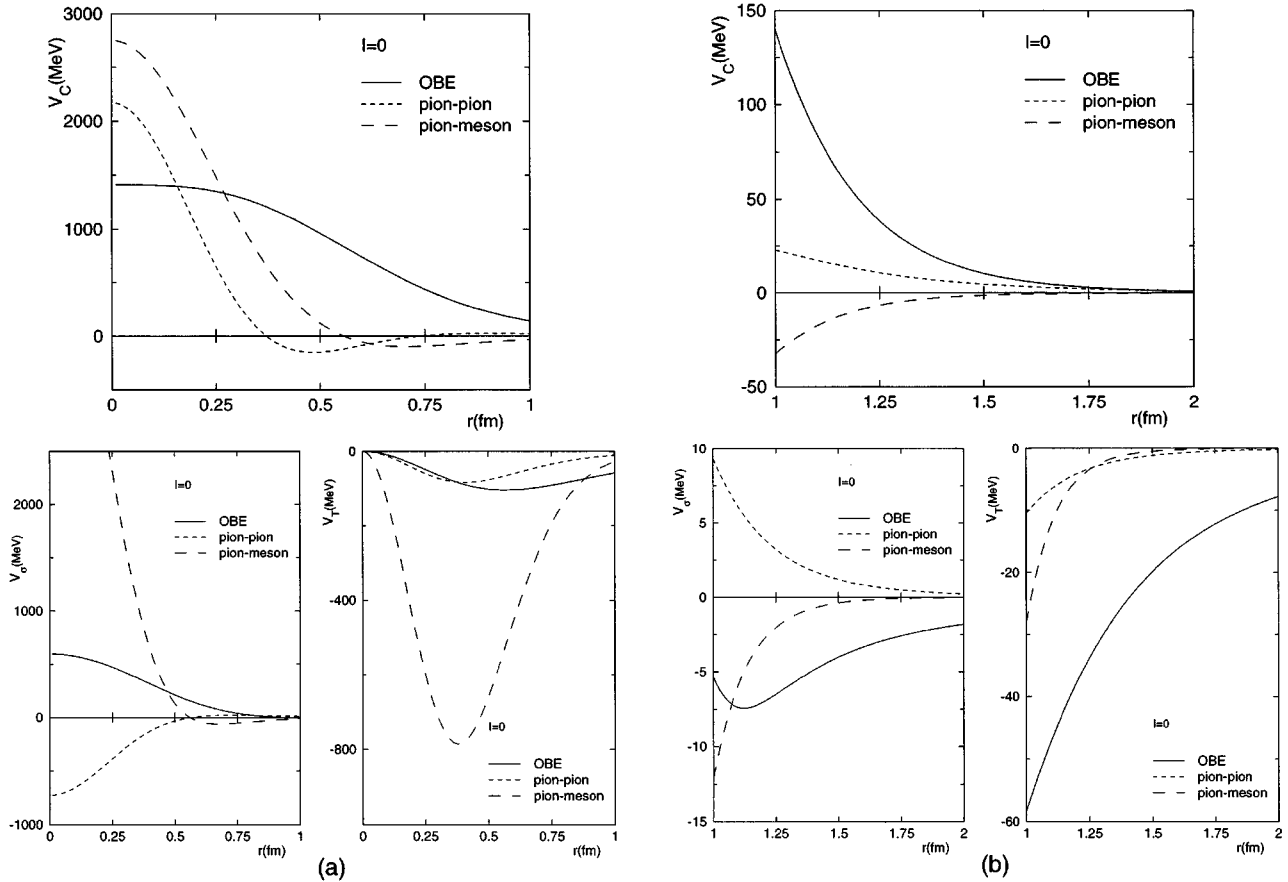


FIG. 3. Central, spin-spin, and tensor potentials for $I=0$. Shown are the one-boson exchange (OBE), the pion-pion exchange, and the other pion-meson exchanges. All potentials are for (a) $r \leq 1$ fm and (b) $1 \leq r \leq 2$ fm. The spin-spin pion-meson potential has its maximum at 4874 MeV.

values of a preliminary version of the Nijmegen extended soft-core (ESC) potential which, next to the standard one-boson exchanges and the two-meson exchanges discussed in this paper, also contains the pair-meson exchanges to be discussed in the following paper [1]. In this model, the pion-nucleon coupling constant at the pion pole was fixed at $f_{NN\pi}^2/4\pi = 0.0745$, in accordance with the recommended value [27]. Keeping in line with the philosophy of the Nijmegen group [2,12,13], we use SU(3) relations for the coupling constants. However, since the existence of a scalar nonet (and hence its quark content) is still controversial, the three nucleon-nucleon-scalar coupling constants are fitted independently. To further limit the number of free parameters, the value for $(f/g)_\rho$ was fixed at the vector-meson dominance value of 3.71. The result of $(f/g)_\omega = -0.06$ is also found to be very close to the vector-meson dominance value of -0.12 , but is not expected to hold exactly since the ϕ meson is not considered to be a pure $s\bar{s}$ system (we do not assume ideal mixing for the vector mesons). It is also interesting to note that the ε coupling constant is much smaller than in the one-boson-exchange Nijm93 potential [13], which is to be expected since in the present ESC model two-pion exchanges are explicitly included. The 14 free parameters are fitted to the 1993 Nijmegen representation of the χ^2 hypersurface of the NN scattering data below $T_{\text{lab}} = 350$ MeV [28], updated with the inclusion of new data which have been published since then. A comparison between this updated partial-wave analysis and the Nijm93 and

ESC potentials will be given in the companion paper [1].

In Figs. 3 and 4, we compare the contributions from one-boson exchange, pion-pion exchange, and the other pion-meson exchanges, all for isospin $I=0$ and $I=1$, respectively. The OBE contributions are the standard OBE potentials, substituting the coupling constants and cutoff masses as given in Table IV. Clearly, these OBE contributions are different from what one would obtain in a potential model containing *only* OBE contributions: The presence of the two-meson contributions substantially modifies the short-range behavior which has to be compensated for. Hence, the OBE contributions of the present ESC model on their own will certainly not fit the data. All potentials are seen to level off towards moderate values at the origin. This is due to the Gaussian form factors. (Note that the Gaussian form factors ensure that all potentials are finite at the origin to all orders in \mathbf{k}^2/M^2 and that the tensor components always vanish at the origin; this in contrast to a monopole or dipole form factor.) The pion-meson contributions dominate the inner region, especially the spin-spin potential, which is mainly due to pion-vector exchange (see Figs. 5 and 6). For $I=1$ the one-boson and pion-pion central contributions cancel each other to a large extent, whereas for $I=0$ they enhance each other. The OBE contributions clearly dominate the outer region ($r \geq 1$ fm).

In Figs. 5 and 6, we compare the contributions to the pion-meson potentials from the different types of mesons: pseudoscalar (π , η , η'), vector (ρ , ω , ϕ), scalar (a_0 , ε ,

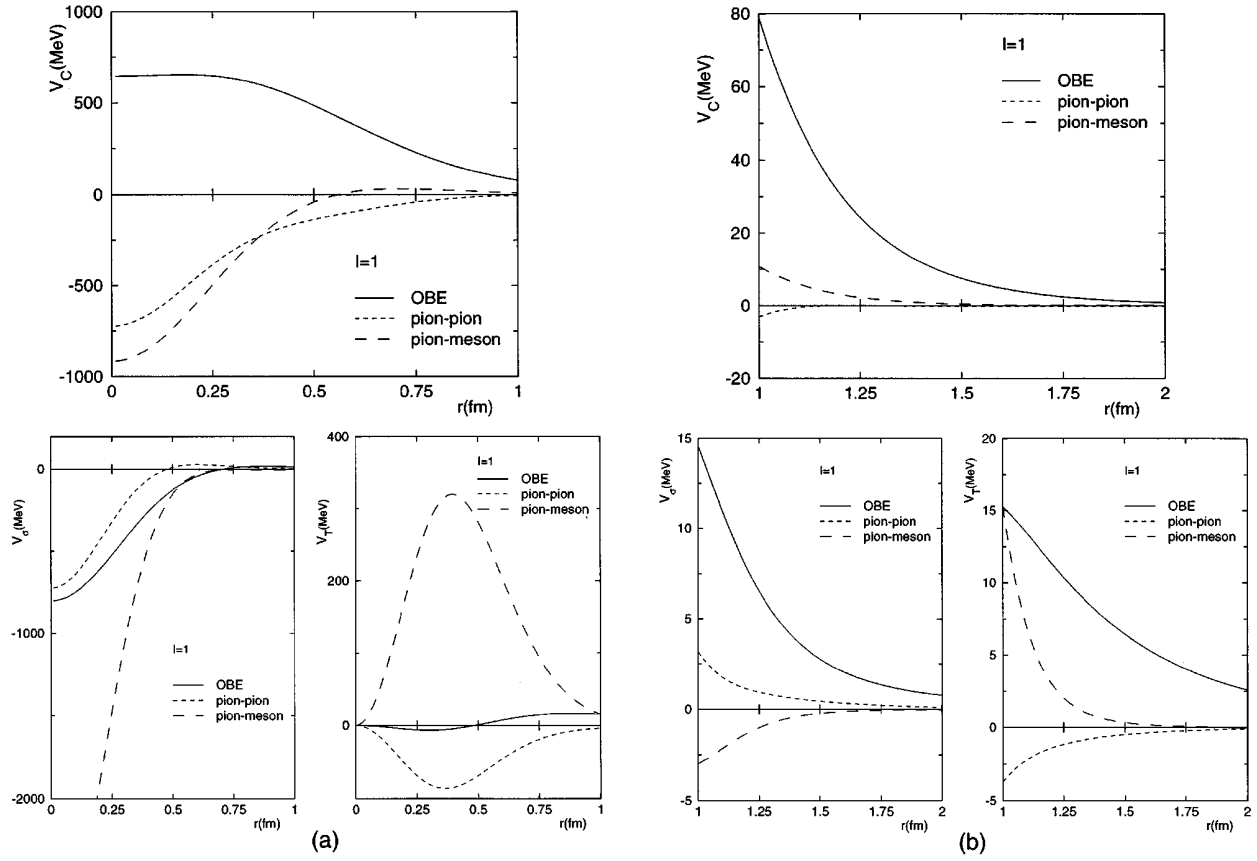


FIG. 4. Same as Fig. 3, but for $I=1$. The spin-spin pion-meson potential has its minimum at -2969 MeV.

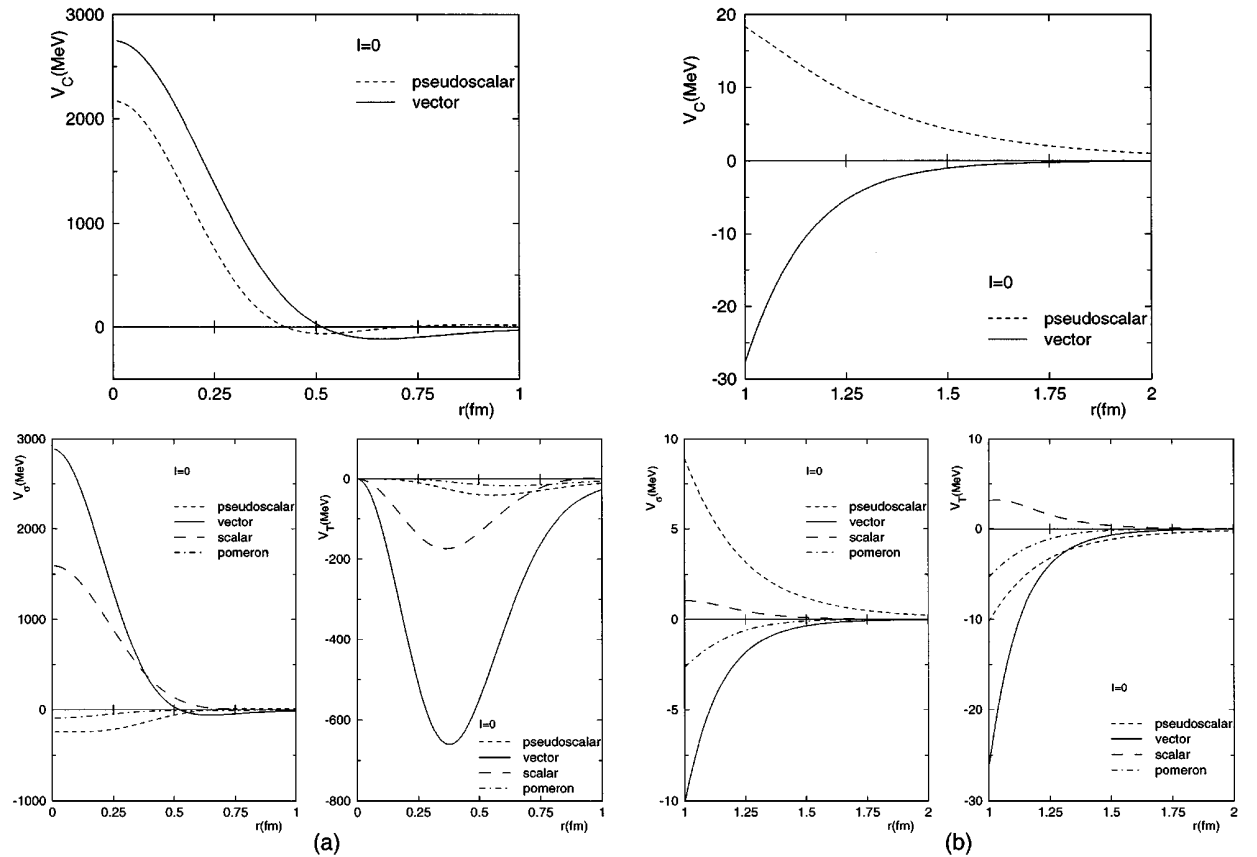
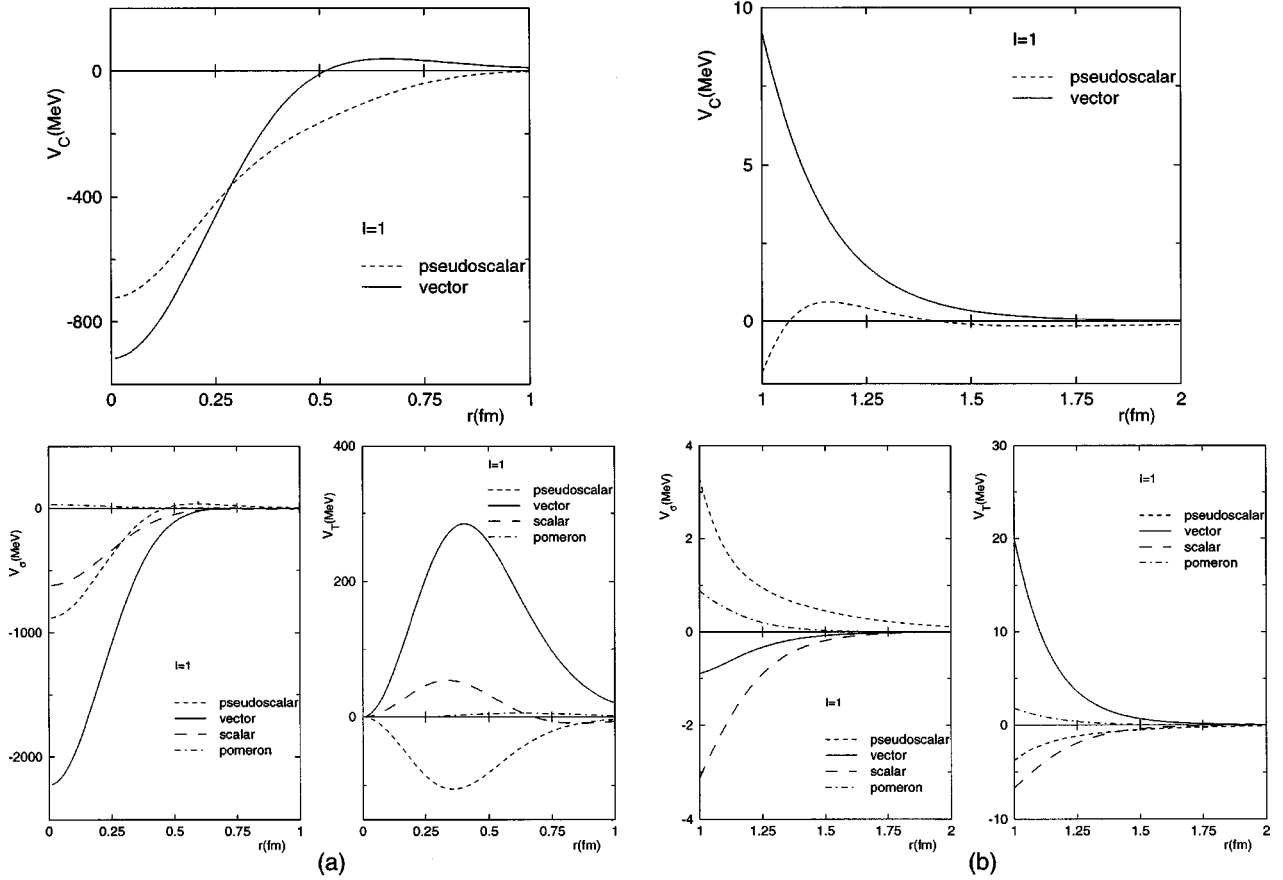


FIG. 5. Central, spin-spin, and tensor potentials for $I=0$. Shown are the pion-pseudoscalar, pion-vector, pion-scalar, and pion-Pomeron exchanges. All potentials are for (a) $r \leq 1$ fm and (b) $1 \leq r \leq 2$ fm.

FIG. 6. Same as Fig. 5, but for $I=1$.

f_0), and Pomeron. The pion-scalar and pion-Pomeron potentials do not have a central component, while the central component of the $\pi\eta$ and $\pi\eta'$ potentials is very small, as can be inferred from the comparison of the pseudoscalar curve in Figs. 5 and 6 and the pion-pion curve in Figs. 3 and 4, respectively. A similar comparison for the spin-spin and tensor components shows that, at short distances, the $\pi\eta$ and $\pi\eta'$ potentials oppose the $\pi\pi$ potentials for $I=0$, resulting in a largely reduced pion-pseudoscalar contribution. For $I=1$ they slightly enhance the $\pi\pi$ potentials. Looking into even more detail (not shown in the figures), we find that the $\pi\eta$ and $\pi\eta'$ potentials are the least important. This is due to the small $NN\eta$ and $NN\eta'$ coupling constants and the high mass of the η' .

The large spin-spin pion-vector potential can be traced to the rather large ω coupling constant and cutoff mass. At the origin, the $\pi\omega$ component reaches a maximum of 3122 MeV for $I=0$, which is only partially reduced by the $\pi\rho$ component. For $I=1$ the $\pi\omega$ component reaches a minimum of -1040 MeV, which enhances the equally large $\pi\rho$ component. The $\pi\phi$ component contributes much less, as is to be expected due to the large ϕ -meson mass. At present, it is not yet clear to us why the model apparently requires such a large spin-spin component.

Comparing our results to those of Holinde and Machleidt (HM) [10] we also find a large cancellation between the $\pi\pi$ and $\pi\rho$ potentials. The cancellation between the $\pi\varepsilon$ and $\pi\omega$ potentials, however, is much less pronounced. One reason for this is the enormous difference in coupling constants:

We have $g_\varepsilon^2/4\pi=0.34$ and $g_\omega^2/4\pi=11$, whereas HM use 6 and 23, respectively. As a matter of fact, in our model the contribution of the $\pi\varepsilon$ potential is almost negligible. Another reason for the only partial cancellation is that we include the scalar f_0 and vector ϕ mesons, whereas HM do not.

The $1/M$ contributions to the potential due to the nonadiabatic, pseudovector-vertex, and off-shell TMO $1/M$ corrections are shown in Fig. 7. Except for the off-shell TMO spin-spin part, all contributions are seen to vanish at the origin. Furthermore, there are large cancellations between the nonadiabatic and pseudovector-vertex corrections, and so the combined $1/M$ contribution to the pion-meson potential is indeed much smaller than the leading-order contribution, validating our procedure of expanding the potential as a series in $1/M$.

In Fig. 8 we show the spin-orbit contributions of the pion-meson potentials in comparison with the spin-orbit OBE potential. The spin-orbit potentials of the pion-scalar and pion-vector exchanges are due to the $1/M^2$ terms in Eqs. (4.13) and (4.26). The spin-orbit pion-pseudoscalar potential, on the other hand, is mainly due to the $1/M$ pseudovector-vertex contributions, and hence is much larger. For $I=1$, the pion-pseudoscalar spin-orbit potential largely cancels the OBE spin-orbit potential in the inner region, whereas for $I=0$ they enhance each other. The resulting spin-orbit part is reduced by the pion-vector spin-orbit contribution. (Incidentally, the large ω coupling constant and cutoff mass might be a necessary condition to arrive at a sufficiently moderate $I=0$

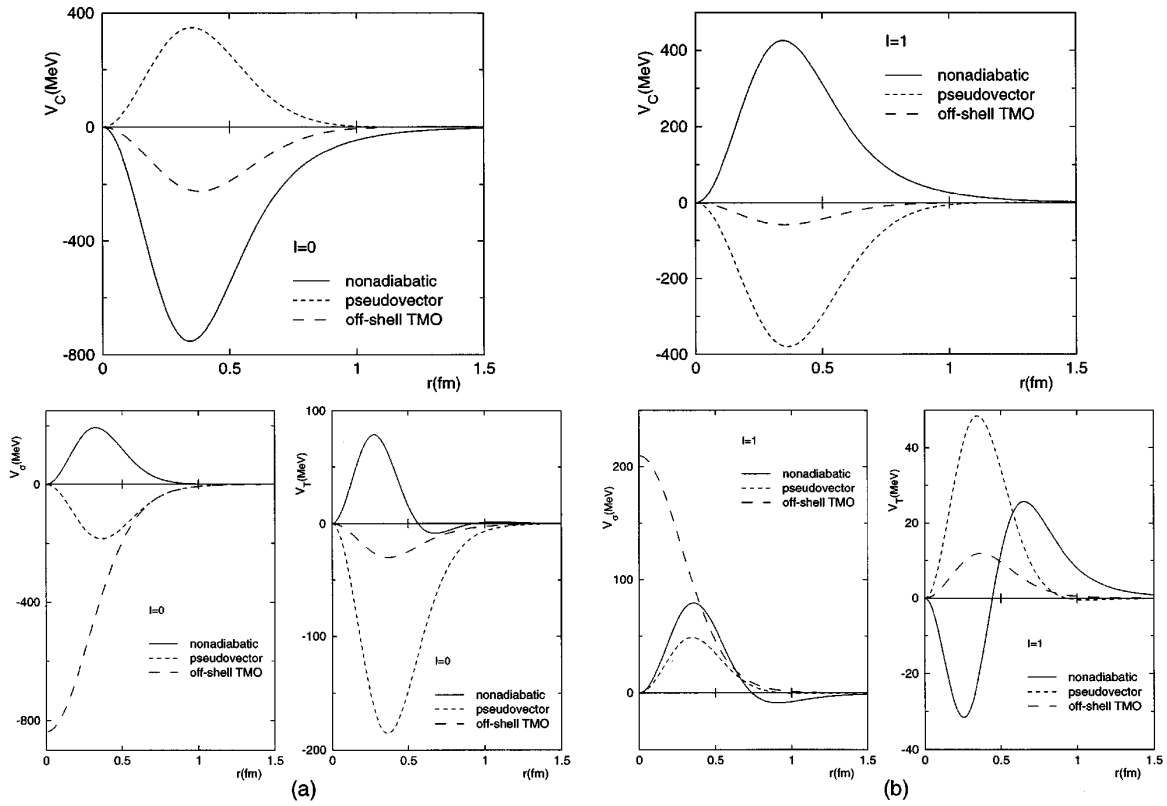


FIG. 7. Nonadiabatic, pseudovector-vertex, and purely off-shell $1/M$ contributions to the pion-meson potentials for (a) $I=0$ and (b) $I=1$.

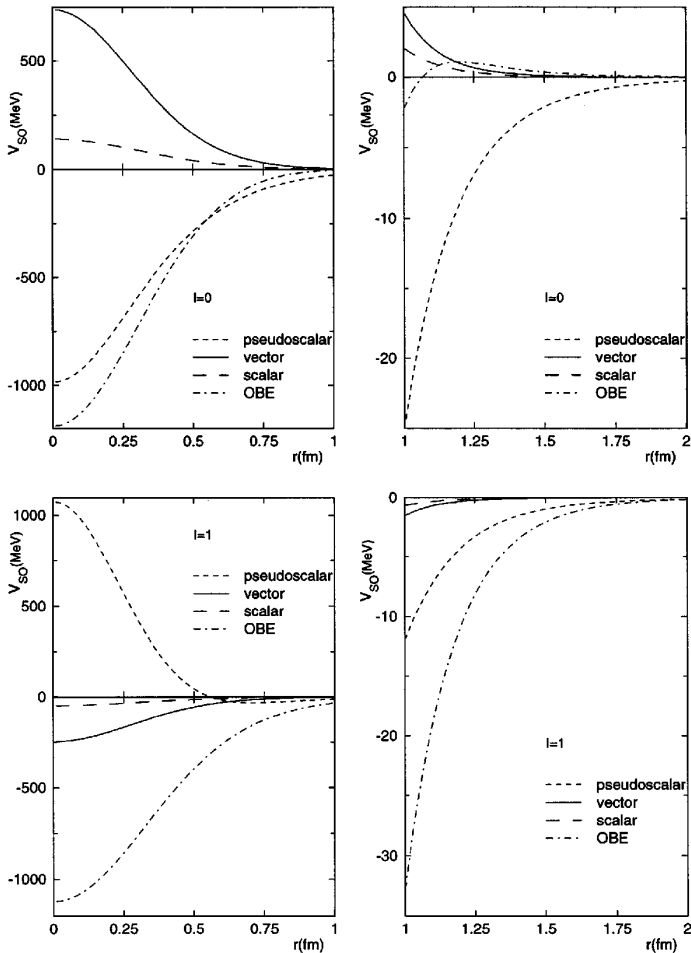


FIG. 8. Spin-orbit contributions of the pion-meson potentials for both $I=0$ and $I=1$ in comparison with the one-boson-exchange contribution.

spin-orbit potential.) On the other hand, the $1/M$ nonadiabatic and off-shell TMO spin-orbit contributions, though much smaller than the pseudovector-vertex contribution, peak near 0.4 fm and, therefore, cause a substantially slower falloff of the spin-orbit component. Because the spin-orbit operator $\mathbf{L} \cdot \mathbf{S}$ is proportional to the angular momentum L , this means that this contribution becomes more and more important for the higher partial waves, i.e., at higher energies. We indeed find that the quality of the fit rapidly becomes worse beyond ~ 300 MeV. It has been argued [29,30] that these spin-orbit contributions will be (partially) canceled by the inclusion of higher-order (three-meson- and four-meson-exchange) diagrams, and so perhaps they should not be included at the present level of our expansion. Alternatively, one can argue that the nonadiabatic expansion in principle breaks down at the pion-production threshold (~ 280 MeV), and so the energy range should not be extended to 350 MeV anyway. However, the inclusion of the nonadiabatic central, spin-spin, and tensor contributions does provide a considerable improvement beyond ~ 280 MeV, apparently contradicting this line of argument. Currently, we are still investigating this matter.

Finally, we note that if we choose to take the pseudoscalar coupling (2.13) instead of the pseudovector coupling (2.12a), there are some small differences in the pion-scalar and pion-vector potentials; i.e., one of the $1/M^2$ terms changes sign (see Table II). A much larger effect is due to the fact that in

case of the pseudoscalar coupling the ω/M pseudovector-vertex corrections of Sec. V B are all absent. Also, there is a sign change in the off-shell TMO corrections, which means that in the pion-pseudoscalar potential the nonadiabatic and off-shell TMO spin-orbit contributions exactly cancel (they have the same r dependence). Hence, the apparent problem with the spin-orbit contribution as discussed above does not occur.

ACKNOWLEDGMENTS

We would like to thank Prof. J.J. de Swart, Prof. I.R. Afnan, and the other members of the theory groups at Nijmegen and Flinders for their stimulating interest. The work of V.S. was financially supported by the Australian Research Council.

APPENDIX A: DIFFERENTIATION DICTIONARY

In this appendix we give a dictionary for the evaluation of the differentiations in Eqs. (4.7), (4.13), (4.26), and the expressions in Sec. V. The procedure is described in more detail in Appendix B of [4]. In the following it is to be understood that the functions on the right-hand side are functions of r and that the prime denotes differentiation with respect to r .

(1) For the pseudoscalar operators $O_{PS}^{(i)}$,

$$\lim_{\mathbf{r}_1 \rightarrow \mathbf{r}_2} (\nabla_1 \cdot \nabla_2)^2 F(r_1) G(r_2) = \frac{2}{r^2} F' G' + F'' G'',$$

$$\lim_{\mathbf{r}_1 \rightarrow \mathbf{r}_2} (\boldsymbol{\sigma}_1 \cdot \nabla_1 \times \nabla_2) (\boldsymbol{\sigma}_2 \cdot \nabla_1 \times \nabla_2) F(r_1) G(r_2) = \frac{2}{3} \left[\frac{1}{r^2} F' G' + \frac{1}{r} F' G'' + \frac{1}{r} F'' G' \right] (\boldsymbol{\sigma}_1 \cdot \boldsymbol{\sigma}_2)$$

$$- \frac{1}{3} \left[\left(F'' - \frac{1}{r} F' \right) \frac{1}{r} G' + \frac{1}{r} F' \left(G'' - \frac{1}{r} G' \right) \right] S_{12}.$$

(2) For the scalar operators $O_S^{(i)}$ and the vector operators $O_{e,e}^{(i)}$, $O_{e,m}^{(i)}$, $O_{e,2m}^{(i)}$, and $O_{m,m}^{(i)}$,

$$\lim_{\mathbf{r}_1 \rightarrow \mathbf{r}_2} (\boldsymbol{\sigma}_1 \cdot \nabla_1) (\boldsymbol{\sigma}_2 \cdot \nabla_1) F(r_1) G(r_2) = \frac{1}{3} \left[\left(F'' + \frac{2}{r} F' \right) G (\boldsymbol{\sigma}_1 \cdot \boldsymbol{\sigma}_2) + \left(F'' - \frac{1}{r} F' \right) G S_{12} \right],$$

$$\lim_{\mathbf{r}_1 \rightarrow \mathbf{r}_2} (\boldsymbol{\sigma}_1 \cdot \nabla_1) (\boldsymbol{\sigma}_2 \cdot \nabla_1) \nabla_2^2 F(r_1) G(r_2) = \frac{1}{3} \left[\left(F''' + \frac{2}{r} F'' \right) \left(G'' + \frac{2}{r} G' \right) (\boldsymbol{\sigma}_1 \cdot \boldsymbol{\sigma}_2) + \left(F'' - \frac{1}{r} F' \right) \left(G'' + \frac{2}{r} G' \right) S_{12} \right],$$

$$\lim_{\mathbf{r}_1 \rightarrow \mathbf{r}_2} (\boldsymbol{\sigma}_1 \cdot \nabla_1) (\boldsymbol{\sigma}_2 \cdot \nabla_1) (\nabla_1 \cdot \nabla_2) F(r_1) G(r_2) = \frac{1}{3} \left[\left(F''' + \frac{2}{r} F'' - \frac{2}{r^2} F' \right) G' (\boldsymbol{\sigma}_1 \cdot \boldsymbol{\sigma}_2) + \left(F''' - \frac{1}{r} F'' + \frac{1}{r^2} F' \right) G' S_{12} \right],$$

$$\lim_{\mathbf{r}_1 \rightarrow \mathbf{r}_2} (\boldsymbol{\sigma}_1 \cdot \nabla_1) (\boldsymbol{\sigma}_2 \cdot \nabla_2) \nabla_1^2 F(r_1) G(r_2) = \frac{1}{3} \left[F''' + \frac{2}{r} F'' - \frac{2}{r^2} F' \right] G' [(\boldsymbol{\sigma}_1 \cdot \boldsymbol{\sigma}_2) + S_{12}],$$

$$\lim_{\mathbf{r}_1 \rightarrow \mathbf{r}_2} (\boldsymbol{\sigma}_1 \cdot \nabla_2) (\boldsymbol{\sigma}_2 \cdot \nabla_1) \nabla_1^2 F(r_1) G(r_2) = \frac{1}{3} \left[F''' + \frac{2}{r} F'' - \frac{2}{r^2} F' \right] G' [(\boldsymbol{\sigma}_1 \cdot \boldsymbol{\sigma}_2) + S_{12}],$$

$$\lim_{\mathbf{r}_1 \rightarrow \mathbf{r}_2} (\boldsymbol{\sigma}_1 \cdot \nabla_1)(\boldsymbol{\sigma}_2 \cdot \nabla_1) \nabla_1^2 F(r_1) G(r_2) = \frac{1}{3} \left[\left(F'''' + \frac{4}{r} F''' \right) G(\boldsymbol{\sigma}_1 \cdot \boldsymbol{\sigma}_2) + \left(F'''' + \frac{1}{r} F''' - \frac{6}{r^2} F'' + \frac{6}{r^3} F' \right) G S_{12} \right],$$

$$\lim_{\mathbf{r}_1 \rightarrow \mathbf{r}_2} [\mathbf{q} \cdot \nabla_1 \times \nabla_2](\boldsymbol{\sigma}_1 + \boldsymbol{\sigma}_2) \cdot \nabla_1 F(r_1) G(r_2) = \frac{2}{r^2} F' G' \mathbf{L} \cdot \mathbf{S}.$$

(3) For the nonadiabatic and pseudovector-vertex corrections,

$$\lim_{\mathbf{r}_1 \rightarrow \mathbf{r}_2} (\nabla_1 \cdot \nabla_2)^3 F(r_1) G(r_2) = \frac{6}{r^2} \left(F'' - \frac{1}{r} F' \right) \left(G'' - \frac{1}{r} G' \right) + F''' G''',$$

$$\begin{aligned} \lim_{\mathbf{r}_1 \rightarrow \mathbf{r}_2} (\nabla_1 \cdot \nabla_2)(\boldsymbol{\sigma}_1 \cdot \nabla_1 \times \nabla_2)(\boldsymbol{\sigma}_2 \cdot \nabla_1 \times \nabla_2) F(r_1) G(r_2) &= -\frac{2}{3} \left[\frac{1}{r^2} \left(\frac{1}{r} F' - F'' + r F''' \right) \left(\frac{1}{r} G' - G'' + r G''' \right) - F''' G''' \right] (\boldsymbol{\sigma}_1 \cdot \boldsymbol{\sigma}_2) \\ &+ \frac{1}{3} \left[\frac{1}{r^2} \left(\frac{2}{r} F' - 2F'' + \frac{r}{2} F''' \right) \left(\frac{2}{r} G' - 2G'' + \frac{r}{2} G''' \right) - \frac{1}{4} F''' G''' \right] S_{12}, \end{aligned}$$

$$\lim_{\mathbf{r}_1 \rightarrow \mathbf{r}_2} (\nabla_1 \cdot \nabla_2)(\boldsymbol{\sigma}_1 + \boldsymbol{\sigma}_2) \cdot (\nabla_1 \times \nabla_2) [\mathbf{q} \cdot (\nabla_1 - \nabla_2)] F(r_1) G(r_2) = -\frac{4}{r^2} \left(F'' - \frac{1}{r} F' \right) \left(G'' - \frac{1}{r} G' \right) \mathbf{L} \cdot \mathbf{S},$$

$$\lim_{\mathbf{r}_1 \rightarrow \mathbf{r}_2} (\boldsymbol{\sigma}_1 \cdot \nabla_1)(\boldsymbol{\sigma}_2 \cdot \nabla_2) F(r_1) G(r_2) = \frac{1}{3} F' G' [(\boldsymbol{\sigma}_1 \cdot \boldsymbol{\sigma}_2) + S_{12}],$$

$$\lim_{\mathbf{r}_1 \rightarrow \mathbf{r}_2} (\boldsymbol{\sigma}_1 \cdot \nabla_2)(\boldsymbol{\sigma}_2 \cdot \nabla_1) F(r_1) G(r_2) = \frac{1}{3} F' G' [(\boldsymbol{\sigma}_1 \cdot \boldsymbol{\sigma}_2) + S_{12}],$$

$$\lim_{\mathbf{r}_1 \rightarrow \mathbf{r}_2} (\boldsymbol{\sigma}_1 + \boldsymbol{\sigma}_2) \cdot \mathbf{q} \times (\nabla_1 + \nabla_2)(\nabla_1 \cdot \nabla_2) F(r_1) G(r_2) = -\frac{2}{r} [F'' G' + F' G''] \mathbf{L} \cdot \mathbf{S},$$

$$\lim_{\mathbf{r}_1 \rightarrow \mathbf{r}_2} (\boldsymbol{\sigma}_1 + \boldsymbol{\sigma}_2) \cdot (\nabla_1 \times \nabla_2) [\mathbf{q} \cdot (\nabla_1 - \nabla_2)] F(r_1) G(r_2) = -\frac{4}{r^2} F' G' \mathbf{L} \cdot \mathbf{S}.$$

APPENDIX B: COORDINATE-SPACE POTENTIALS

In this appendix we give the explicit expressions for the coordinate-space two-meson-exchange potentials. We also include the result for the two-pion-exchange potential from Ref. [3] for reasons of completeness. In order to keep the expressions as compact as possible, we restrict ourselves to the leading-order terms (no $1/M^2$ contributions), and define \odot and \otimes operations as

$$(F \odot G)_\sigma(r) = \frac{1}{3} \left(F'' + \frac{2}{r} F' \right) G(r),$$

$$(F \odot G)_T(r) = \frac{1}{3} \left(F'' - \frac{1}{r} F' \right) G(r),$$

$$(F \otimes G)_C(r) = \left[F'' G'' + \frac{2}{r^2} F' G' \right] (r),$$

$$(F \otimes G)_\sigma(r) = \frac{2}{3} \left[\frac{1}{r^2} F' G' + \frac{1}{r} F'' G' + \frac{1}{r} F' G'' \right] (r),$$

$$(F \otimes G)_T(r) = \frac{1}{3} \left[\frac{2}{r^2} F' G' - \frac{1}{r} F'' G' - \frac{1}{r} F' G'' \right] (r).$$

We then find the following [$F_\alpha(\lambda, r)$ is given by Eq. (4.5)].

(1) Pseudoscalar exchanges:

$$\begin{aligned} V(\pi\pi) &= -\left(\frac{f_{NN\pi}}{m_\pi} \right)^4 \frac{2}{\pi} \int_0^\infty \frac{d\lambda}{\lambda^2} \\ &\times \{ 2(\boldsymbol{\tau}_1 \cdot \boldsymbol{\tau}_2) [(I_2^\pi \otimes I_2^\pi)_C - (F_\pi \otimes F_\pi)_C] \\ &+ 3[(I_2^\pi \otimes I_2^\pi)_\sigma - (F_\pi \otimes F_\pi)_\sigma] (\boldsymbol{\sigma}_1 \cdot \boldsymbol{\sigma}_2) \\ &+ 3[(I_2^\pi \otimes I_2^\pi)_T - (F_\pi \otimes F_\pi)_T] S_{12} \}, \end{aligned} \quad (\text{B1})$$

$$\begin{aligned} V(\pi\eta) &= -2 \left(\frac{f_{NN\eta}}{m_\pi} \right)^2 \left(\frac{f_{NN\pi}}{m_\pi} \right)^2 (\boldsymbol{\tau}_1 \cdot \boldsymbol{\tau}_2) \frac{2}{\pi} \int_0^\infty \frac{d\lambda}{\lambda^2} \\ &\times \{ [(I_2^\pi \otimes I_2^\eta)_\sigma - (F_\pi \otimes F_\eta)_\sigma] (\boldsymbol{\sigma}_1 \cdot \boldsymbol{\sigma}_2) \\ &+ [(I_2^\pi \otimes I_2^\eta)_T - (F_\pi \otimes F_\eta)_T] S_{12} \}, \end{aligned} \quad (\text{B2})$$

$$V(\pi\eta') = V(\pi\eta) \quad \text{with } \eta \rightarrow \eta'. \quad (\text{B3})$$

(2) Scalar exchanges:

$$V(\pi a_0) = 4g_{a_0}^2 \left(\frac{f_{NN\pi}}{m_\pi} \right)^2 (\boldsymbol{\tau}_1 \cdot \boldsymbol{\tau}_2) \frac{2}{\pi} \int_0^\infty \frac{d\lambda}{\lambda^2} \\ \times \{ [(I_2^\pi \odot I_2^{a_0})_\sigma - (F_\pi \odot F_{a_0})_\sigma] (\boldsymbol{\sigma}_1 \cdot \boldsymbol{\sigma}_2) \\ + [(I_2^\pi \odot I_2^{a_0})_T - (F_\pi \odot F_{a_0})_T] S_{12} \}, \quad (\text{B4})$$

$$V(\pi \varepsilon) = V(\pi f_0) = 0. \quad (\text{B5})$$

(3) Pomeron exchange:

$$V(\pi P) = 0. \quad (\text{B6})$$

(4) Vector exchanges:

$$V(\pi \rho) = -4g_\rho^2 \left(\frac{f_{NN\pi}}{m_\pi} \right)^2 (\boldsymbol{\tau}_1 \cdot \boldsymbol{\tau}_2) \frac{2}{\pi} \int_0^\infty \frac{d\lambda}{\lambda^2} \\ \times \{ [(I_2^\pi \odot I_2^\rho)_\sigma - (F_\pi \odot F_\rho)_\sigma] (\boldsymbol{\sigma}_1 \cdot \boldsymbol{\sigma}_2) \\ + [(I_2^\pi \odot I_2^\rho)_T - (F_\pi \odot F_\rho)_T] S_{12} \}, \quad (\text{B7})$$

$$V(\pi \omega) = V(\pi \phi) = 0. \quad (\text{B8})$$

-
- [1] Th.A. Rijken and V.G.J. Stoks, Phys. Rev. C **54**, 2869 (1996), the following paper.
- [2] M.M. Nagels, Th.A. Rijken, and J.J. de Swart, Phys. Rev. D **17**, 768 (1978).
- [3] Th.A. Rijken, Ann. Phys. (N.Y.) **208**, 253 (1991).
- [4] Th.A. Rijken and V.G.J. Stoks, Phys. Rev. C **46**, 73 (1992).
- [5] Th.A. Rijken and V.G.J. Stoks, Phys. Rev. C **46**, 102 (1992).
- [6] S. Weinberg, Phys. Lett. B **251**, 288 (1990); Nucl. Phys. **B363**, 3 (1991); C. Ordóñez and U. van Kolck, Phys. Lett. B **291**, 459 (1992).
- [7] R. Dolen, D. Horn, and C. Schmid, Phys. Rev. **166**, 1768 (1968); H. Harari, Phys. Rev. Lett. **20**, 1395 (1968); F.J. Gilman, H. Harari, and Y. Zarmi, *ibid.* **21**, 323 (1968).
- [8] Although the existence of the scalar nonet is still controversial, there appears to be evidence for a scalar–isoscalar resonant state $0^{++}(750)$; see M. Svec, A. de Lesquen, and L. van Rossum, Phys. Rev. D **46**, 949 (1992) and M. Svec, *ibid.* **53**, 2343 (1996).
- [9] D.O. Riska, Nucl. Phys. **A274**, 349 (1976).
- [10] K. Holinde and R. Machleidt, Nucl. Phys. **A372**, 349 (1981).
- [11] E. Salpeter, Phys. Rev. **87**, 328 (1952).
- [12] P.M.M. Maessen, Th.A. Rijken, and J.J. de Swart, Phys. Rev. C **40**, 2226 (1989).
- [13] V.G.J. Stoks, R.A.M. Klomp, C.P.F. Terheggen, and J.J. de Swart, Phys. Rev. C **49**, 2950 (1994).
- [14] R.B. Wiringa, Phys. Rev. C **43**, 1585 (1991).
- [15] S.C. Pieper, R.B. Wiringa, and V.R. Pandharipande, Phys. Rev. C **46**, 1741 (1992).
- [16] S. Takeuchi, K. Shimizu, and K. Yazaki, Nucl. Phys. **A504**, 777 (1989).
- [17] F. Fernández, A. Valarce, U. Straub, and A. Faessler, J. Phys. G **19**, 2013 (1993).
- [18] K.A. Brueckner and K.M. Watson, Phys. Rev. **92**, 1023 (1953).
- [19] M. Taketani, S. Machida, and S. Ohnuma, Progr. Theor. Phys. (Kyoto) **7**, 45 (1952).
- [20] J.L. Friar and S.A. Coon, Phys. Rev. C **49**, 1272 (1994).
- [21] We follow the conventions of J.D. Bjorken and S.D. Drell, *Relativistic Quantum Mechanics and Relativistic Quantum Fields* (McGraw-Hill Inc., New York, 1965).
- [22] F.E. Low, Phys. Rev. D **12**, 163 (1975).
- [23] S. Nussinov, Phys. Rev. Lett. **34**, 1286 (1975); Phys. Rev. D **14**, 246 (1976).
- [24] Yu.A. Simonov, Phys. Lett. B **249**, 514 (1990).
- [25] Th.A. Rijken, Ph.D. thesis, University of Nijmegen, 1975 (unpublished); Th.A. Rijken, Ann. Phys. (N.Y.) **164**, 1, 23 (1985).
- [26] L. Durand, Phys. Rev. Lett. **18**, 58 (1967); L. van Hove, Phys. Lett. **24B**, 183 (1967).
- [27] V. Stoks, R. Timmermans, and J.J. de Swart, Phys. Rev. C **47**, 512 (1993).
- [28] V.G.J. Stoks, R.A.M. Klomp, M.C.M. Rentmeester, and J.J. de Swart, Phys. Rev. C **48**, 792 (1993).
- [29] A. Klein, Phys. Rev. **90**, 1101 (1953).
- [30] M.M. Lévy, Phys. Rev. **88**, 72 (1952); **88**, 725 (1952).